SepONet: Efficient Large-Scale Physics-Informed Operator Learning

Xinling Yu[1, *], **Sean Hooten** [2, *], **Ziyue Liu**[1], **Yequan Zhao**[1], **Marco Fiorentino**[2], **Thomas Van Vaerenbergh**[3], **Zheng Zhang**[1]
[1] University of California, Santa Barbara
[2] Hewlett Packard Labs, Hewlett Packard Enterprise
[3] Hewlett Packard Labs, HPE Belgium
[*] Equal Contributions

Abstract

We introduce Separable Operator Networks (SepONet), a novel framework that significantly enhances the efficiency of physics-informed operator learning. SepONet uses independent trunk networks to learn basis functions separately for different coordinate axes, enabling faster and more memory-efficient training via forward-mode automatic differentiation. We provide a universal approximation theorem for SepONet proving that it generalizes to arbitrary operator learning problems, and then validate its performance through comprehensive benchmarking against physics-informed DeepONet. Our results demonstrate SepONet's superior performance across various nonlinear and inseparable PDEs, with SepONet's advantages increasing with problem complexity, dimension, and scale. Open source code is available at `https://github.com/HewlettPackard/separable-operator-networks`.

1 Introduction

Operator learning, which aims to learn mappings between infinite-dimensional function spaces, has emerged as a powerful tool in scientific machine learning for modeling complex physical systems (30; 25; 24; 26). This approach has been successfully applied to climate modeling (15; 36), multiphysics simulation (29; 3; 33; 27; 20), inverse design (32; 9), and various other fields (14; 12; 42; 10). Deep Operator Networks (DeepONets) (30) stand out due to their universal approximation guarantee (4) and robustness (31). Physics-informed deep operator networks (PI-DeepONet) (43) further enhance this approach by incorporating physics constraints, eliminating the need for ground-truth output functions. However, PI-DeepONet training is memory-intensive and time-consuming, particularly due to the computation of high-order derivatives across multiple PDE configurations.

To address these inefficiencies, we propose Separable Operator Networks (SepONet), inspired by the separation of variables technique in solving PDEs and recent work on separable PINN (6). Our key contributions are:

- We introduce SepONet, a physics-informed operator learning framework that significantly enhances scaling efficiency in terms of training time and GPU memory usage, enabling extreme-scale learning of continuous mappings between infinite-dimensional function spaces.
- We provide a theoretical foundation for SepONet through the universal approximation theorem, proving its capability to approximate any nonlinear continuous operator with arbitrary accuracy.
- We validate our theoretical results through benchmarking SepONet against PI-DeepONet on a range of 1D and 2D time-dependent PDEs, demonstrating SepONet's efficiency in largr-scale learning of nonlinear and inseparable PDEs.

D3S3: Data-driven and Differentiable Simulations, Surrogates, and Solvers @ NeurIPS 2024.

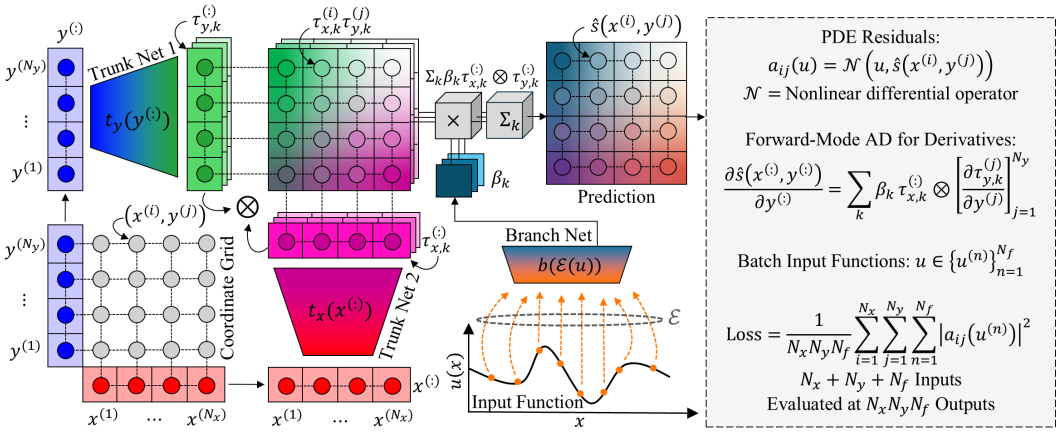

Figure 1: Separable operator network (SepONet) architecture for 2D problem instance. A coordinate grid of collocation points $(x^{(i)}, y^{(j)})$ can be evaluated efficiently by separating the coordinate axes, feeding them through independent trunk networks, and combining the outputs by outer product to obtain multiple basis function maps. Meanwhile, the branch network processes input functions and outputs coefficients, which are then used to scale and combine the trunk network basis functions by product and sum. Spatiotemporal derivatives of the output predictions are obtained efficiently by forward automatic differentiation due to the independence of trunk networks.

Our results show up to 112× training speed-up for 1D time-dependent PDEs with minimal memory increase. Notably, SepONet operates efficiently with less than 1GB of GPU memory in scenarios where PI-DeepONet exhausts 80GB. Furthermore, SepONet scales efficiently with problem dimension, enabling accurate prediction of 2D time-dependent PDEs at scales where PI-DeepONet fails.

2 Separable Operator Networks (SepONet)

In this work we propose separable operator networks (SepONet), which learns basis functions separately for different coordinate axes as shown in Fig. 1. SepONet approximates the solution operator of a PDE system parameterized by u for any given point $y = (y_1, \ldots, y_d)$ as:

$$G_{\boldsymbol{\theta}}(u)(y_1, \ldots, y_d) = \sum_{k=1}^{r} \beta_k \prod_{n=1}^{d} \tau_{n,k} = b_\psi(\mathcal{E}(u)) \cdot \left(t_{\phi_1}^1(y_1) \odot t_{\phi_2}^2(y_2) \odot \cdots \odot t_{\phi_d}^d(y_d)\right), \quad (1)$$

where $\odot$ is the Hadamard (element-wise) vector product and $\cdot$ is the vector dot product. Here, $\mathcal{E}$ is the encoder mapping the input function u to its point-wise evaluations and $\beta_k = b_\psi(\mathcal{E}(u))_k$ is the k-th output of the branch net, as in DeepONet. However, unlike DeepONet, which employs a single trunk net that processes each collocation point y individually, SepONet uses d independent trunk nets, $t_{\phi_n}^n : \mathbb{R} \to \mathbb{R}^r$ for $n = 1, \ldots, d$. In particular, $\tau_{n,k} = t_{\phi_n}^n(y_n)_k$ denotes the k-th output of the n-th trunk net. Importantly, the parameters of the n-th trunk net ϕ_n are independent of all other trunk net parameter sets. This allows for efficient, parallelized computation of high-order derivatives via forward-mode automatic differentiation. The parameters of SepONet, $\boldsymbol{\theta} = (\psi, \phi_1, \ldots, \phi_d)$, are then updated using backpropagation. For detailed information on the operator learning problem definition and SepONet implementation, please refer to Appendix A and Appendix B, respectively.

Universal Approximation Property of SepONet We present the universal approximation theorem to show that proposed separable operator networks can approximate any nonlinear continuous operators that map infinite-dimensional function spaces to others.

Theorem 1 (Universal Approximation Theorem for Separable Operator Networks)**.** *Suppose that σ is a Tauber-Wiener function, g is a sinusoidal function, $\mathcal{X}$ is a Banach space, $K \subseteq \mathcal{X}$, $K_1 \subseteq \mathbb{R}^{d_1}$ and $K_2 \subseteq \mathbb{R}^{d_2}$ are three compact sets in $\mathcal{X}$, $\mathbb{R}^{d_1}$ and $\mathbb{R}^{d_2}$, respectively, $\mathcal{U}$ is a compact set in $C(K)$, G is a nonlinear continuous operator, which maps $\mathcal{U}$ into a compact set $\mathcal{S} \subseteq C(K_1 \times K_2)$, then for any $\epsilon > 0$, there are positive integers n, r, m, constants c_i^k, ζ_k^1, ζ_k^2, ξ_{ij}^k, $\theta_i^k \in \mathbb{R}$, points $\omega_k^1 \in \mathbb{R}^{d_1}$,*

$\omega_k^2 \in \mathbb{R}^{d_2}$, $x_j \in K$, $i = 1, \ldots, n$, $k = 1, \ldots, r$, $j = 1, \ldots, m$, *such that*

$$\left| G(u)(y) - \sum_{k=1}^{r} \underbrace{\sum_{i=1}^{n} c_i^k \sigma \left(\sum_{j=1}^{m} \xi_{ij}^k u\left(x_j\right) + \theta_i^k \right)}_{branch} \underbrace{g\left(w_k^1 \cdot y_1 + \zeta_k^1\right)}_{trunk_1} \underbrace{g\left(w_k^2 \cdot y_2 + \zeta_k^2\right)}_{trunk_2} \right| < \epsilon \quad (2)$$

holds for all $u \in \mathcal{U}$, $y = (y_1, y_2) \in K_1 \times K_2$.

Proof. The proof can be found in Appendix C.2. □

Remark. *Here we show the approximation property of a separable operator network with two trunk nets. By repeatedly applying trigonometric angle addition formula, it is trivial to separate* y *as* $(y_1, y_2, \ldots, y_d) \in K_1 \times K_2 \times \ldots \times K_d$ *and extend Eq.* (2) *to* d *trunk nets.*

3 Numerical Results

This section presents comprehensive numerical studies demonstrating the expressive power and effectiveness of SepONet compared to PI-DeepONet on various time-dependent PDEs: diffusion-reaction, advection, Burgers', and (2+1)-dimensional nonlinear diffusion equations. We set the number of residual points $N_r = N^d = N_c$, for problem dimension d and integer N. N_c will be referred to as the number of training points. The number of initial and boundary points per axis is set to $N_I = N_b = N = \sqrt[d]{N_c}$. We evaluate both models by varying the number of input functions (N_f) and training points (N_c) across four key perspectives: test accuracy, GPU memory usage, training time, and large-scale learning capabilities. The main results are illustrated in Fig. 2 and Fig. 3, with complete test results reported in Appendix D.4. PDE definitions, training details, and problem-specific parameters are provided in Appendix D.1 and Appendix D.2.

Test Accuracy Both PI-DeepONet and SepONet demonstrate improved accuracy when increasing either the number of training points (N_c) or the number of input functions (N_f), while fixing the other parameter. This trend is consistent across all four equations tested.

GPU Memory Usage The models' GPU memory usage patterns differ significantly, particularly evident in the advection equation case. When varying N_c from 8^2 to 128^2 (fixing $N_f = 100$), PI-DeepONet's GPU memory consumption rises steeply from 0.967 GB to 59.806 GB. In contrast, SepONet maintains a low, constant footprint between 0.713 GB and 0.719 GB. Similar patterns emerge when varying N_f from 5 to 100 (fixing $N_c = 128^2$): PI-DeepONet's usage escalates from 3.021 GB to 59.806 GB, while SepONet remains stable.

Training Time Training time scaling mirrors GPU memory usage patterns. For the advection equation, as N_c increases from 8^2 to 128^2 (fixing $N_f = 100$), PI-DeepONet's training time rises from 0.0787 to 8.231 hours, while SepONet remains steady between 0.0730 and 0.0843 hours. When varying N_f from 5 to 100 (fixing $N_c = 128^2$), PI-DeepONet's time increases from 0.3997 to 8.231 hours, whereas SepONet maintains times between 0.0730 and 0.0754 hours. This demonstrates SepONet's superior scalability in training time, a crucial advantage for large-scale applications.

Large-scale Learning The Burgers' and nonlinear diffusion equations demonstrate SepONet's capabilities in extreme-scale scenarios. For the Burgers' equation, PI-DeepONet reaches its limit at $N_c = 64^2$ with a 13.72% relative ℓ_2 error, while SepONet achieves 7.51% error at $N_c = 128^2$ (Fig. 2(c)). The nonlinear diffusion equation further highlights this difference: PI-DeepONet fails due to memory constraints, whereas SepONet efficiently handles $N_c = 128^3$ and $N_f = 100$, achieving a 6.44% error (Fig. 3(d)). Additional SepONet scaling results up to $N_c = 512^2$ and $N_f = 800$ for Burgers' equation are provided in Appendix D.3.

4 Conclusion

In conclusion, Separable Operator Networks (SepONet) present a promising solution to the challenges faced in operator learning. By balancing data efficiency and computational resource management,

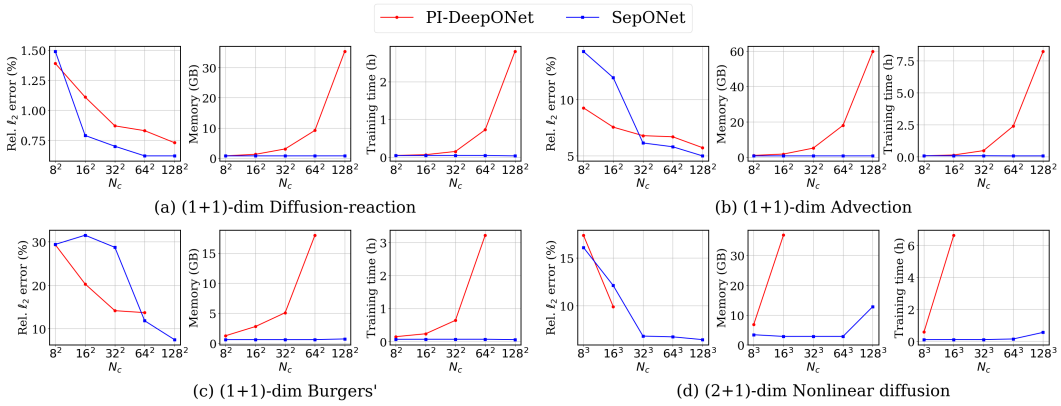

Figure 2: Performance comparison of PI-DeepONet and SepONet with varying number of training points (N_c) and fixed number of input functions ($N_f = 100$).

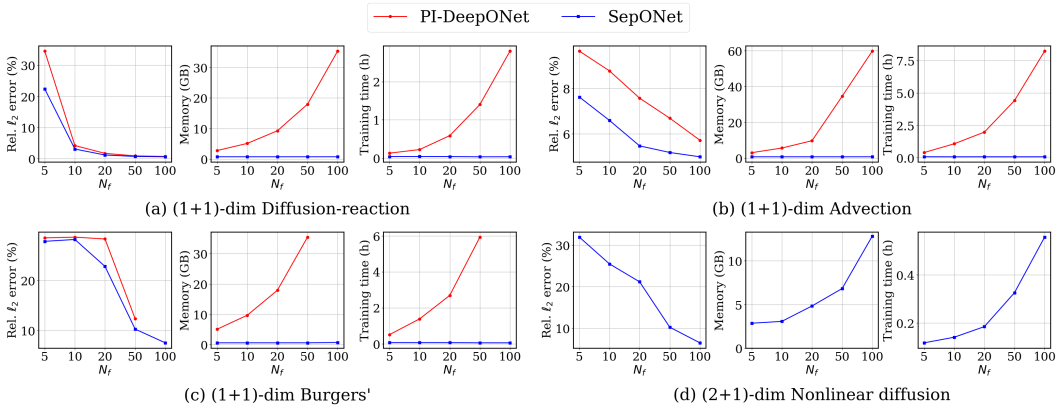

Figure 3: Performance comparison of PI-DeepONet and SepONet with increasing number of input functions (N_f) and fixed number of training points ($N_c = 128^d$, where d is the problem dimension). Note: PI-DeepONet results for the (2+1)-dimensional diffusion equation are unavailable due to memory constraints.

SepONet offers a novel approach that addresses the limitations of both DeepONets and PI-DeepONets. Its basis function construction method, grounded in universal approximation theory, enables accurate modeling of complex, nonlinear systems while maintaining computational efficiency through forward-mode automatic differentiation. While SepONet demonstrates significant advantages, future research directions include adapting the method for irregular geometries (23; 41; 8), exploring nonlinear decoder implementations (40), and investigating neural scaling laws in physics-informed operator learning. These advancements will further expand SepONet's applicability and effectiveness across a broader range of physical problems.

Acknowledgments

We would like to thank Wolfger Peelaers for the valuable discussions and insightful comments.

References

[1] A. G. Baydin, B. A. Pearlmutter, A. A. Radul, and J. M. Siskind, *Automatic differentiation in machine learning: a survey*, Journal of machine learning research, 18 (2018), pp. 1–43.

[2] J. BRADBURY, R. FROSTIG, P. HAWKINS, M. J. JOHNSON, C. LEARY, D. MACLAURIN, G. NECULA, A. PASZKE, J. VANDERPLAS, S. WANDERMAN-MILNE, AND Q. ZHANG, *JAX: composable transformations of Python+NumPy programs*, 2018, `http://github.com/google/jax`.

[3] S. CAI, Z. WANG, L. LU, T. A. ZAKI, AND G. E. KARNIADAKIS, *Deepm&mnet: Inferring the electroconvection multiphysics fields based on operator approximation by neural networks*, Journal of Computational Physics, 436 (2021), p. 110296.

[4] T. CHEN AND H. CHEN, *Universal approximation to nonlinear operators by neural networks with arbitrary activation functions and its application to dynamical systems*, IEEE transactions on neural networks, 6 (1995), pp. 911–917.

[5] P.-H. CHIU, J. C. WONG, C. OOI, M. H. DAO, AND Y.-S. ONG, *Can-pinn: A fast physics-informed neural network based on coupled-automatic–numerical differentiation method*, Computer Methods in Applied Mechanics and Engineering, 395 (2022), p. 114909.

[6] J. CHO, S. NAM, H. YANG, S.-B. YUN, Y. HONG, AND E. PARK, *Separable physics-informed neural networks*, Advances in Neural Information Processing Systems, 36 (2024).

[7] T. A. DRISCOLL, N. HALE, AND L. N. TREFETHEN, *Chebfun guide*, 2014.

[8] Z. FANG, S. WANG, AND P. PERDIKARIS, *Learning only on boundaries: a physics-informed neural operator for solving parametric partial differential equations in complex geometries*, Neural Computation, 36 (2024), pp. 475–498.

[9] J. GU, Z. GAO, C. FENG, H. ZHU, R. CHEN, D. BONING, AND D. PAN, *Neurolight: A physics-agnostic neural operator enabling parametric photonic device simulation*, Advances in Neural Information Processing Systems, 35 (2022), pp. 14623–14636.

[10] J. K. GUPTA AND J. BRANDSTETTER, *Towards multi-spatiotemporal-scale generalized pde modeling*, arXiv preprint arXiv:2209.15616, (2022).

[11] D. HE, S. LI, W. SHI, X. GAO, J. ZHANG, J. BIAN, L. WANG, AND T.-Y. LIU, *Learning physics-informed neural networks without stacked back-propagation*, in International Conference on Artificial Intelligence and Statistics, PMLR, 2023, pp. 3034–3047.

[12] R. HWANG, J. Y. LEE, J. Y. SHIN, AND H. J. HWANG, *Solving pde-constrained control problems using operator learning*, in Proceedings of the AAAI Conference on Artificial Intelligence, vol. 36, 2022, pp. 4504–4512.

[13] A. ISERLES, *A first course in the numerical analysis of differential equations*, no. 44, Cambridge university press, 2009.

[14] Z. JIANG, M. ZHU, D. LI, Q. LI, Y. O. YUAN, AND L. LU, *Fourier-mionet: Fourier-enhanced multiple-input neural operators for multiphase modeling of geological carbon sequestration*, arXiv preprint arXiv:2303.04778, (2023).

[15] K. KASHINATH, M. MUSTAFA, A. ALBERT, J. WU, C. JIANG, S. ESMAEILZADEH, K. AZIZZADENESHELI, R. WANG, A. CHATTOPADHYAY, A. SINGH, ET AL., *Physics-informed machine learning: case studies for weather and climate modelling*, Philosophical Transactions of the Royal Society A, 379 (2021), p. 20200093.

[16] K. A. KHAN AND P. I. BARTON, *A vector forward mode of automatic differentiation for generalized derivative evaluation*, Optimization Methods and Software, 30 (2015), pp. 1185–1212.

[17] P. KIDGER AND C. GARCIA, *Equinox: neural networks in JAX via callable PyTrees and filtered transformations*, Differentiable Programming workshop at Neural Information Processing Systems 2021, (2021).

[18] D. P. KINGMA AND J. BA, *Adam: A method for stochastic optimization*, arXiv preprint arXiv:1412.6980, (2014).

[19] D. KOCHKOV, J. A. SMITH, A. ALIEVA, Q. WANG, M. P. BRENNER, AND S. HOYER, *Machine learning–accelerated computational fluid dynamics*, Proceedings of the National Academy of Sciences, 118 (2021), p. e2101784118.

[20] K. KONTOLATI, S. GOSWAMI, G. EM KARNIADAKIS, AND M. D. SHIELDS, *Learning nonlinear operators in latent spaces for real-time predictions of complex dynamics in physical systems*, Nature Communications, 15 (2024), p. 5101.

[21] N. B. KOVACHKI, S. LANTHALER, AND H. MHASKAR, *Data complexity estimates for operator learning*, arXiv preprint arXiv:2405.15992, (2024).

[22] S. LANTHALER, S. MISHRA, AND G. E. KARNIADAKIS, *Error estimates for deeponets: A deep learning framework in infinite dimensions*, Transactions of Mathematics and Its Applications, 6 (2022), p. tnac001.

[23] Z. LI, D. Z. HUANG, B. LIU, AND A. ANANDKUMAR, *Fourier neural operator with learned deformations for pdes on general geometries*, Journal of Machine Learning Research, 24 (2023), pp. 1–26.

[24] Z. LI, N. KOVACHKI, K. AZIZZADENESHELI, B. LIU, K. BHATTACHARYA, A. STUART, AND A. ANANDKUMAR, *Fourier neural operator for parametric partial differential equations*, arXiv preprint arXiv:2010.08895, (2020).

[25] Z. LI, N. KOVACHKI, K. AZIZZADENESHELI, B. LIU, K. BHATTACHARYA, A. STUART, AND A. ANANDKUMAR, *Neural operator: Graph kernel network for partial differential equations*, arXiv preprint arXiv:2003.03485, (2020).

[26] Z. LI, H. ZHENG, N. KOVACHKI, D. JIN, H. CHEN, B. LIU, K. AZIZZADENESHELI, AND A. ANANDKUMAR, *Physics-informed neural operator for learning partial differential equations*, ACM/JMS Journal of Data Science, 1 (2024), pp. 1–27.

[27] C. LIN, Z. LI, L. LU, S. CAI, M. MAXEY, AND G. E. KARNIADAKIS, *Operator learning for predicting multiscale bubble growth dynamics*, The Journal of Chemical Physics, 154 (2021).

[28] H. LIU, H. YANG, M. CHEN, T. ZHAO, AND W. LIAO, *Deep nonparametric estimation of operators between infinite dimensional spaces*, arXiv preprint arXiv:2201.00217, (2022).

[29] Z. LIU, Y. LI, J. HU, X. YU, S. SHIAU, X. AI, Z. ZENG, AND Z. ZHANG, *Deepoheat: operator learning-based ultra-fast thermal simulation in 3d-ic design*, in 2023 60th ACM/IEEE Design Automation Conference (DAC), IEEE, 2023, pp. 1–6.

[30] L. LU, P. JIN, G. PANG, Z. ZHANG, AND G. E. KARNIADAKIS, *Learning nonlinear operators via deeponet based on the universal approximation theorem of operators*, Nature machine intelligence, 3 (2021), pp. 218–229.

[31] L. LU, X. MENG, S. CAI, Z. MAO, S. GOSWAMI, Z. ZHANG, AND G. E. KARNIADAKIS, *A comprehensive and fair comparison of two neural operators (with practical extensions) based on fair data*, Computer Methods in Applied Mechanics and Engineering, 393 (2022), p. 114778.

[32] L. LU, R. PESTOURIE, S. G. JOHNSON, AND G. ROMANO, *Multifidelity deep neural operators for efficient learning of partial differential equations with application to fast inverse design of nanoscale heat transport*, Physical Review Research, 4 (2022), p. 023210.

[33] Z. MAO, L. LU, O. MARXEN, T. A. ZAKI, AND G. E. KARNIADAKIS, *Deepm&mnet for hypersonics: Predicting the coupled flow and finite-rate chemistry behind a normal shock using neural-network approximation of operators*, Journal of computational physics, 447 (2021), p. 110698.

[34] C. C. MARGOSSIAN, *A review of automatic differentiation and its efficient implementation*, Wiley interdisciplinary reviews: data mining and knowledge discovery, 9 (2019), p. e1305.

[35] R. S. PALANI, *spinop.m (spin operator)*. `https://www.mathworks.com/matlabcentral/fileexchange/71536-spinop-m-spin-operator`, 2024. MATLAB Central File Exchange. Retrieved June 28, 2024.

[36] J. PATHAK, S. SUBRAMANIAN, P. HARRINGTON, S. RAJA, A. CHATTOPADHYAY, M. MARDANI, T. KURTH, D. HALL, Z. LI, K. AZIZZADENESHELI, ET AL., *Fourcastnet: A global data-driven high-resolution weather model using adaptive fourier neural operators*, arXiv preprint arXiv:2202.11214, (2022).

[37] S. B. POPE, *Turbulent flows*, Measurement Science and Technology, 12 (2001), pp. 2020–2021.

[38] M. RAISSI, P. PERDIKARIS, AND G. E. KARNIADAKIS, *Physics-informed neural networks: A deep learning framework for solving forward and inverse problems involving nonlinear partial differential equations*, Journal of Computational physics, 378 (2019), pp. 686–707.

[39] M. SEEGER, *Gaussian processes for machine learning*, International journal of neural systems, 14 (2004), pp. 69–106.

[40] J. SEIDMAN, G. KISSAS, P. PERDIKARIS, AND G. J. PAPPAS, *Nomad: Nonlinear manifold decoders for operator learning*, Advances in Neural Information Processing Systems, 35 (2022), pp. 5601–5613.

[41] L. SERRANO, L. LE BOUDEC, A. KASSAÏ KOUPAÏ, T. X. WANG, Y. YIN, J.-N. VITTAUT, AND P. GALLINARI, *Operator learning with neural fields: Tackling pdes on general geometries*, Advances in Neural Information Processing Systems, 36 (2024).

[42] K. SHUKLA, V. OOMMEN, A. PEYVAN, M. PENWARDEN, L. BRAVO, A. GHOSHAL, R. M. KIRBY, AND G. E. KARNIADAKIS, *Deep neural operators can serve as accurate surrogates for shape optimization: a case study for airfoils*, arXiv preprint arXiv:2302.00807, (2023).

[43] S. WANG, H. WANG, AND P. PERDIKARIS, *Learning the solution operator of parametric partial differential equations with physics-informed deeponets*, Science advances, 7 (2021), p. eabi8605.

[44] K. WEIERSTRASS, *Über die analytische darstellbarkeit sogenannter willkürlicher functionen einer reellen veränderlichen*, Sitzungsberichte der Königlich Preußischen Akademie der Wissenschaften zu Berlin, 2 (1885), p. 364.

A Preliminaries

A.1 Operator Learning for Solving Parametric Partial Differential Equations

Let $\mathcal{X}$ and $\mathcal{Y}$ be Banach spaces, with $K \subseteq \mathcal{X}$ and $K_1 \subseteq \mathcal{Y}$ being compact sets. Consider a nonlinear continuous operator $G : \mathcal{U} \to \mathcal{S}$, mapping functions from one infinite-dimensional space to another, where $\mathcal{U} \subseteq C(K)$ and $\mathcal{S} \subseteq C(K_1)$. The goal of operator learning is to approximate the operator G using a model parameterized by $\boldsymbol{\theta}$, denoted as $G_{\boldsymbol{\theta}}$. Here, $\mathcal{U}$ and $\mathcal{S}$ represent spaces of functions where the input and output functions have dimensions d_u and d_s, respectively. We focus on the scalar case where $d_u = d_s = 1$ throughout this paper without loss of generality, however, it should be noted that the results apply to arbitrary d_u and d_s.

In the context of solving parametric partial differential equations (PDEs), consider PDEs of the form:

$$\mathcal{N}(u, s) = 0,\ \mathcal{I}(u, s) = 0,\ \mathcal{B}(u, s) = 0, \tag{3}$$

where $\mathcal{N}$ is a nonlinear differential operator, $\mathcal{I}$ and $\mathcal{B}$ represent the initial and boundary conditions, $u \in \mathcal{U}$ denotes the PDE configurations (source terms, coefficients, initial conditions, and etc.), and $s \in \mathcal{S}$ denotes the corresponding PDE solution. Assuming that for any $u \in \mathcal{U}$ there exists a unique solution $s \in \mathcal{S}$, we can define the solution operator $G : \mathcal{U} \to \mathcal{S}$ as $s = G(u)$.

A widely used framework for approximating such an operator G involves constructing $G_{\boldsymbol{\theta}}$ through three maps (22):

$$G_{\boldsymbol{\theta}} \approx G := \mathcal{D} \circ \mathcal{A} \circ \mathcal{E}. \tag{4}$$

First, the encoder $\mathcal{E} : \mathcal{U} \to \mathbb{R}^m$ maps an input function $u \in \mathcal{U}$ to a finite-dimensional feature representation. Next, the approximator $\mathcal{A} : \mathbb{R}^m \to \mathbb{R}^r$ transforms this encoded data within the finite-dimensional space $\mathbb{R}^m$ to another finite-dimensional space $\mathbb{R}^r$. Finally, the decoder $\mathcal{D} : \mathbb{R}^r \to \mathcal{S}$ produces the output function $s(y) = G(u)(y)$ for $y \in K_1$.

A.2 Deep Operator Networks (DeepONet)

The original DeepONet formulation (30) can be analyzed through the 3-step approximation framework Eq. (4). The encoder $\mathcal{E} : \mathcal{U} \to \mathbb{R}^m$ maps the input function u to its point-wise evaluations at m fixed sensors $x_1, x_2, \ldots, x_m \in K$, e.g., $(u(x_1), ..., u(x_m)) = \mathcal{E}(u)$. Two separate neural networks (usually multilayer perceptrons), the branch net and the trunk net, serve as the approximator and decoder, respectively. The branch net $b_\psi : \mathbb{R}^m \to \mathbb{R}^r$ parameterized by ψ processes $(u(x_1), \ldots, u(x_m))$ to produce a feature embedding $(\beta_1, \beta_2, \ldots, \beta_r)$. The trunk net $t_\phi : \mathbb{R}^d \to \mathbb{R}^r$ with parameters ϕ, takes a continuous coordinate $y = (y_1, ..., y_d)$ as input and outputs a feature embedding $(\tau_1, \tau_2, \ldots, \tau_r)$. The final DeepONet prediction of a function u for a query y is:

$$G_{\boldsymbol{\theta}}(u)(y) = \sum_{k=1}^{r} \beta_k \tau_k = b_\psi(\mathcal{E}(u)) \cdot t_\phi(y), \tag{5}$$

where $\cdot$ is the vector dot product and $\boldsymbol{\theta} = (\psi, \phi)$ represents all the trainable parameters in the branch and trunk nets.

Despite DeepONet's remarkable success across a range of applications in multiphysics simulation (3; 33; 27), inverse design (32), and carbon storage (14), its supervised training process is highly dependent on the availability of training data, which can be costly. Indeed, the generalization error of DeepONets scales with the number of training input-output function pairs (30; 21; 28). Generating a large number of high-quality training data is expensive or even impractical in some applications. For example, in simulating high Reynolds number (Re) turbulent flow (37), accurate numerical simulations require a fine mesh, leading to a computational cost scaling with Re^3 (19), making the generation of sufficiently large and diverse training datasets prohibitively expensive.

To address the need for costly data acquisition, physics-informed deep operator networks (PI-DeepONet) (43), inspired by physics-informed neural networks (PINNs) (38), have been proposed to learn operators without relying on observed input-output function pairs. Given a dataset of N_f input training functions, N_r residual points, N_I initial points, and N_b boundary points: $\mathcal{D} = \left\{ \{u^{(i)}\}_{i=1}^{N_f}, \{y_r^{(j)}\}_{j=1}^{N_r}, \{y_I^{(j)}\}_{j=1}^{N_I}, \{y_b^{(j)}\}_{j=1}^{N_b} \right\}$, PI-DeepONets are trained by minimizing an unsupervised physics loss:

$$L_{physics}(\boldsymbol{\theta}|\mathcal{D}) = L_{residual}(\boldsymbol{\theta}|\mathcal{D}) + \lambda_I L_{initial}(\boldsymbol{\theta}|\mathcal{D}) + \lambda_b L_{boundary}(\boldsymbol{\theta}|\mathcal{D}), \tag{6}$$

where

$$\begin{aligned} L_{residual}(\boldsymbol{\theta}|\mathcal{D}) &= \frac{1}{N_f N_r} \sum_{i=1}^{N_f} \sum_{j=1}^{N_r} \left| \mathcal{N}(u^{(i)}, G_{\boldsymbol{\theta}}(u^{(i)})(y_r^{(j)})) \right|^2, \\ L_{initial}(\boldsymbol{\theta}|\mathcal{D}) &= \frac{1}{N_f N_I} \sum_{i=1}^{N_f} \sum_{j=1}^{N_I} \left| \mathcal{I}(u^{(i)}, G_{\boldsymbol{\theta}}(u^{(i)})(y_I^{(j)})) \right|^2, \\ L_{boundary}(\boldsymbol{\theta}|\mathcal{D}) &= \frac{1}{N_f N_b} \sum_{i=1}^{N_f} \sum_{j=1}^{N_b} \left| \mathcal{B}(u^{(i)}, G_{\boldsymbol{\theta}}(u^{(i)})(y_b^{(j)})) \right|^2. \end{aligned} \tag{7}$$

Here, λ_I and λ_b denote the weight coefficients for different loss terms. However, as noted in the original PI-DeepONet paper (43), the training process can be both memory-intensive and time-consuming. Similar to PINNs (38), this inefficiency arises because optimizing the physics loss requires calculating high-order derivatives of the PDE solution with respect to numerous collocation points, typically achieved via reverse-mode automatic differentiation (1). This process involves backpropagating the physics loss through the unrolled computational graph to update the model parameters. For PI-DeepONet, the inefficiency is even more pronounced, as the physics loss terms (Eq. (7)) must be evaluated across multiple PDE configurations. Although various works (5; 11; 6) have proposed different methods to improve the training efficiency of PINNs, little research has focused on enhancing the training efficiency of PI-DeepONet. We propose to address this inefficiency through a separation of input variables.

A.3 Separation of Variables

The method of separation of variables seeks solutions to PDEs of the form $s(y) = T(t)Y_1(y_1) \cdots Y_d(y_d)$ for an input point $y = (t, y_1, \ldots, y_d)$ and univariate functions $T, Y_1, \ldots, Y_d$.

Suppose we have a linear PDE system

$$\mathcal{M}[t]s(y) = \mathcal{L}_1[y_1]s(y) + \cdots + \mathcal{L}_d[y_d]s(y), \tag{8}$$

where $\mathcal{M}[t] = \frac{d}{dt} + h(t)$ is a first order differential operator of t, and $\mathcal{L}_1[y_1], ..., \mathcal{L}_d[y_d]$ are linear second order ordinary differential operators of their respective variables $y_1, ..., y_d$ only. Furthermore, assume we are provided Robin boundary conditions in each variable and separable initial condition $s(t = 0, y_1, \ldots, y_d) = \prod_{n=1}^{d} \phi_n(y_n)$ for functions $\phi_n(y_n)$ that satisfy the boundary conditions. Then, leveraging Sturm-Liouville theory and some massaging, the solution to this problem can be written

$$s(y) = s(t, y_1, \ldots, y_d) = \sum_k A_k T^k(t) \prod_{n=1}^{d} Y_n^k(y_n), \tag{9}$$

where k is a lumped index that counts over infinite eigenfunctions of each $\mathcal{L}_i$ operator (potentially with repeats). For example, given $n \in \{1, ..., d\}$, $\mathcal{L}_n Y_n^k(y_n) = \lambda_n^k Y_n^k$ for eigenvalue $\lambda_n^k \in \mathbb{R}$. $T^k(t)$ depends on all the eigenvalues λ_n^k corresponding to index k. $A_k \in \mathbb{R}$ is a coefficient determined by the initial condition. More details can be found in Appendix E. The method of separation of variables applied to a heat equation example can be found in supplemental materials.

One may notice the resemblance between the form of the DeepONet prediction Eq. (5) with Eq. (9), provided $\beta_k = A_k$ and $\tau_k = T^k(t) \prod_{i=1}^{d} Y_i^k(y_i)$, with appropriately ordered k. We leverage this similarity explicitly in the construction of SepONet below.

B SepONet Implementation Details

Suppose we are provided a computation domain $K_1 = [0, 1]^d$ of dimension d, and an input function u. Let $N_r = N^d$ for given integer N. To make predictions along N^d collocation points, PI-DeepONet must directly sample all N^d points: $\{y^{(i)}\}_{i=1}^{N^d} = \{y_1^{(i)}, ..., y_d^{(i)}\}_{i=1}^{N^d}$ where $y^{(i)} \in K_1$ for any i. By contrast, to compute predictions at $N_r = N^d$ collocation points, SepONet only needs to sample N points along each coordinate axis, e.g. $\{\{y_1^{(i)}\}_{i=1}^{N}, ..., \{y_d^{(i)}\}_{i=1}^{N}\}$, for a total of dN samples.

For shorthand and generality, we will denote the dataset of input points for SepONet as $\mathcal{D} = \{y_1^{(:)}, \ldots, y_d^{(:)}\}$. Each $y_n^{(:)} = \{y_n^{(i)}\}_{i=1}^{N_n}$ represents an array of N_n samples along the n-th coordinate axis for a total of $\sum_{n=1}^{d} N_n$ samples. The initial and boundary points may be separately sampled from ∂K_1; the number of samples (N_I and N_b) and sampling strategy are equivalent for SepONet and PI-DeepONet.

B.1 Forward Pass

The forward pass of SepONet, illustrated for $d = 2$ in Fig. 1, follows the formulation Eq. (1) except generalized to the practical setting where predictions along a grid of collocation points are processed in parallel. The formula can be expressed:

$$\begin{aligned} G_{\boldsymbol{\theta}}(u)(y_1^{(:)}, \ldots, y_d^{(:)}) &= \sum_{k=1}^{r} \beta_k \bigotimes_{n=1}^{d} \tau_{n,k}^{(:)} \\ &= \sum_{k=1}^{r} b_\psi(\mathcal{E}(u))_k \left(t_{\phi_1}^1(y_1^{(:)})_k \otimes t_{\phi_2}^2(y_2^{(:)})_k \otimes \cdots \otimes t_{\phi_d}^d(y_d^{(:)})_k \right), \end{aligned} \tag{10}$$

where $\otimes$ is the (outer) tensor product, which produces an output predictive array along a meshgrid of $N_1 \times N_2 \times \cdots \times N_d$ collocation points. Notably, $\tau_{n,k}^{(:)} = t_{\phi_n}^n(y_n^{(:)})_k$ represents a vector of N_n values produced by the n-th trunk net along the k-th output mode after feeding all $y_n^{(:)}$ points. After taking the outer product along each of $n = 1, \ldots, d$ dimensions for all r modes, the modes are sum-reduced with the predictions of the branch net $\beta_k = b_\psi(\mathcal{E}(u))_k$. While not shown here, our implementation also batches over input functions $\{u^{(i)}\}_{i=1}^{N_f}$ for N_f functions. Thus, for only $N_f + N_1 + \cdots + N_d$ inputs, SepONet produces a predictive array with shape $N_f \times N_1 \times \cdots \times N_d$.

B.2 Model Update

In evaluation of the physics loss Eq. (6), SepONet enables more efficient computation of high-order derivatives in terms of both time and memory use compared to PI-DeepONet by leveraging forward-mode automatic differentiation (AD) (16). This is fairly evident by the form of Eq. (10). For example, to compute derivatives along all inputs of the m-th axis

$$\frac{\partial G_\theta(u)(y_1^{(:)}, ..., y_d^{(:)})}{\partial y_m^{(:)}} = \sum_{k=1}^{r} \beta_k \left(\bigotimes_{n \neq m} \tau_{n,k}^{(:)} \right) \otimes \left[\frac{\partial \tau_{m,k}}{\partial y_m} \right]^{(:)} \tag{11}$$

$$\left[\frac{\partial \tau_{m,k}}{\partial y_m} \right]^{(:)} := \left[\frac{\partial \tau_{m,k}^{(1)}}{\partial y_m^{(1)}}, \ldots, \frac{\partial \tau_{m,k}^{(N_m)}}{\partial y_m^{(N_m)}} \right]^T, \tag{12}$$

where $\left[\frac{\partial \tau_{m,k}}{\partial y_m} \right]^{(:)}$ is a vector of derivatives of the m-th trunk net's k-th basis function evaluated along all inputs to the m-th coordinate axis. One may notice that Eq. (12) can be written as a Jacobian-vector product of the "Jacobian" of the (m, k)-th trunk net outputs with respect to all $y_m^{(:)}$ inputs with a tangent vector of 1's: $\left[\frac{\partial \tau_{m,k}}{\partial y_m} \right]^{(:)} = \frac{\partial \left(\tau_{m,k}^{(1)}, \ldots, \tau_{m,k}^{(N_m)} \right)}{\partial \left(y_m^{(1)}, \ldots, y_m^{(N_m)} \right)} \mathbf{1}$. This is equivalent to forward-mode AD. Consequently, the derivatives along the m-th coordinate axis across the entire grid of predictions can be obtained by pushing forward derivatives of the m-th trunk net, and then reusing the outputs of all other $n \neq m$ trunk nets via outer product. By contrast, PI-DeepOnet must compute derivatives $\frac{\partial t_\phi(y_1, \ldots, y_d)}{\partial y_m}$ for each input-output pair individually, where there is no such advantage and it is more prudent to use reverse-mode AD. Fundamentally, the advantage of SepONet for using forward-mode AD can be attributed to the significantly smaller input-output relationship when evaluating along coordinate grids $\mathbb{R}^{N_1 + \cdots + N_d} \to \mathbb{R}^{N_1 \cdots N_d}$ compared to PI-DeepONet $\mathbb{R}^{N_1 \cdots N_d} \to \mathbb{R}^{N_1 \cdots N_d}$. For a more detailed explanation of forward- and reverse-mode AD, we refer readers to (6; 34). Once the physics loss is computed, reverse-mode AD is employed to update the model parameters $\theta = (\psi, \phi_1, \ldots, \phi_d)$.

C Universal Approximation Theorem for Separable Operator Networks

Here we present the universal approximation theorem for the proposed separable operator networks, originally written in Theorem 1 and repeated below in Theorem 8. We begin by reviewing established theoretical results on approximating continuous functions and functionals. Following this review, we introduce the preliminary lemmas and proofs necessary for understanding Theorem 8. We refer our readers to (4; 44) for detailed proofs of Theorem 2, Theorem 3, Theorem 4. Main notations are listed in Table 1.

C.1 Preliminaries and Auxiliary Results

Definition (Tauber-Wiener (TW))**.** *If a function $g : \mathbb{R} \to \mathbb{R}$ (continuous or discontinuous) satisfies that all the linear combinations $\sum_{i=1}^{N} c_i g(\lambda_i x + \theta_i)$, $\lambda_i \in \mathbb{R}$, $\theta_i \in \mathbb{R}$, $c_i \in \mathbb{R}$, $i = 1, 2, \ldots, N$, are dense in every $C[a, b]$, then g is called a Tauber-Wiener (TW) function.*

Remark (Density in $C[a, b]$)**.** *A set of functions is said to be dense in $C[a, b]$ if every function in the space of continuous functions on the interval $[a, b]$ can be approximated arbitrarily closely by functions from the set.*

Definition (Compact Set)**.** *Suppose that X is a Banach space, $V \subseteq X$ is called a compact set in X, if for every sequence $\{x_n\}_{n=1}^{\infty}$ with all $x_n \in V$, there is a subsequence $\{x_{n_k}\}$, which converges to some element $x \in V$.*

Theorem 2 ((4))**.** *Suppose that K is a compact set in $\mathbb{R}^n$, $\mathcal{S}$ is a compact set in $C(K)$, $g \in$ (TW), then for any $\epsilon > 0$, there exist a positive integer N, real numbers θ_i, vectors $\omega_i \in \mathbb{R}^n$, $i = 1, \ldots, N$, which are independent of $f \in C(K)$ and constants $c_i(f)$, $i = 1, \ldots, N$ depending on f, such that*

$$\left| f(x) - \sum_{i=1}^{N} c_i(f) g(\omega_i \cdot x + \theta_i) \right| < \epsilon \tag{13}$$

Table 1: Notations and Symbols

X	some Banach space with norm $\|\cdot\|_X$
$\mathbb{R}^d$	Euclidean space of dimension d
K	some compact set in a Banach space
$C(K)$	Banach space of all continuous functions defined on K, with norm $\|f\|_{C(K)} = \max_{x\in K} \|f(x)\|$
$\tilde{C}[a,b]$	the space of functions in $C[a,b]$ satisfying $f(a) = f(b)$
V	some compact set in $C(K)$
$u(x)$	some input function
$\mathcal{U}$	the space of input functions
G	some continuous operator
$G(u)(y)$ or $s(y)$	some output function that is mapped from the corresponding input function u by the operator G
$\mathcal{S}$	the space of output functions
(TW)	all the Tauber-Wiener functions
σ and g	activation function for branch net and trunk nets in Theorem 8
$\{x_1, x_2, \ldots, x_m\}$	m sensor points for identifying input function u
r	rank of some deep operator network or separable operator network
n, m	operator network size hyperparameters in Theorem 8

holds for all $x \in K$ and $f \in \mathcal{S}$. Moreover, each $c_i(f)$ is a linear continuous functional defined on $\mathcal{S}$.

Theorem 3 ((4))**.** *Suppose that $\sigma \in (\mathrm{TW})$, X is a Banach Space, $K \subseteq X$ is a compact set, $\mathcal{U}$ is a compact set in $C(K)$, f is a continuous functional defined on $\mathcal{U}$, then for any $\epsilon > 0$, there are positive integers N, m points $x_1, \ldots, x_m \in K$, and real constants c_i, θ_i, ξ_{ij}, $i = 1, \ldots, N$, $j = 1, \ldots, m$, such that*

$$\left| f(u) - \sum_{i=1}^{N} c_i \sigma \left(\sum_{j=1}^{m} \xi_{ij} u(x_j) + \theta_i \right) \right| < \epsilon \tag{14}$$

holds for all $u \in \mathcal{U}$.

Theorem 4 (Weierstrass Approximation Theorem (44))**.** *Suppose $f \in C[a,b]$, then for every $\epsilon > 0$, there exists a polynomial p such that for all x in $[a,b]$, we have $|f(x) - p(x)| < \epsilon$.*

Corollary 4.1. *Trigonometric polynomials are dense in the space of continuous and periodic functions $\tilde{C}[0, 2\pi] := \{f \in C[0, 2\pi] \mid f(0) = f(2\pi)\}$.*

Proof. For any $\tilde{f} \in \tilde{C}[0, 2\pi]$, extend it to a 2π-periodic and continuous function f defined on $\mathbb{R}$. It suffices to show that there exists a trigonometric polynomial that approximates f within any $\epsilon > 0$. We construct the continuous even functions of 2π period g and h as:

$$g(\theta) = \frac{f(\theta) + f(-\theta)}{2} \quad \text{and} \quad h(\theta) = \frac{f(\theta) - f(-\theta)}{2} \sin(\theta). \tag{15}$$

Let $\phi(x) = g(\arccos x)$ and $\psi(x) = h(\arccos x)$. Since ϕ, ψ are continuous functions on $[-1, 1]$, by the Weierstrass Approximation Theorem Theorem 4, for any $\epsilon > 0$, there exist polynomials p and q such that

$$|\phi(x) - p(x)| < \frac{\epsilon}{4} \quad \text{and} \quad |\psi(x) - q(x)| < \frac{\epsilon}{4} \tag{16}$$

holds for all $x \in [-1, 1]$. Let $x = \cos\theta$, it follows that

$$|g(\theta) - p(\cos\theta)| < \frac{\epsilon}{4} \quad \text{and} \quad |h(\theta) - q(\cos\theta)| < \frac{\epsilon}{4} \tag{17}$$

for $\theta \in [0, \pi]$. Because g, h and $cosine$ are even and 2π-periodic, Eq. (17) holds for all $\theta \in \mathbb{R}$. From the definitions of g and h, and the fact $|\sin\theta| \leq 1$, $\left|\sin^2\theta\right| \leq 1$, we have

$$\left| \frac{f(\theta) + f(-\theta)}{2} \sin^2\theta - p(\cos\theta)\sin^2\theta \right| < \frac{\epsilon}{4} \quad \text{and} \quad \left| \frac{f(\theta) - f(-\theta)}{2} \sin^2\theta - q(\cos\theta)\sin\theta \right| < \frac{\epsilon}{4}. \tag{18}$$

Using the triangle inequality, we obtain

$$\left| f(\theta)\sin^2\theta - \left[p(\cos\theta)\sin^2\theta + q(\cos\theta)\sin\theta \right] \right| < \frac{\epsilon}{2}. \tag{19}$$

Applying the same analysis to

$$\tilde{g}(\theta) = \frac{f(\theta + \frac{\pi}{2}) + f(-\theta + \frac{\pi}{2})}{2} \quad \text{and} \quad \tilde{h}(\theta) = \frac{f(\theta + \frac{\pi}{2}) - f(-\theta + \frac{\pi}{2})}{2} \sin(\theta), \tag{20}$$

we can find polynomials r and s such that

$$\left| f\left(\theta + \frac{\pi}{2}\right) \sin^2\theta - \left[r(\cos\theta)\sin^2\theta + s(\cos\theta)\sin\theta \right] \right| < \frac{\epsilon}{2} \tag{21}$$

holds for all θ. Substituting θ with $\theta - \frac{\pi}{2}$ gives

$$\left| f(\theta)\cos^2\theta - \left[r(\sin\theta)\cos^2\theta - s(\sin\theta)\cos\theta \right] \right| < \frac{\epsilon}{2}. \tag{22}$$

By the triangle inequality, combining Eq. (22) and Eq. (19) gives

$$\left| f(\theta) - \left[r(\sin\theta)\cos^2\theta - s(\sin\theta)\cos\theta + p(\cos\theta)\sin^2\theta + q(\cos\theta)\sin\theta \right] \right| < \epsilon \tag{23}$$

holds for all θ. Thus, the trigonometric polynomial

$$r(\sin\theta)\cos^2\theta - s(\sin\theta)\cos\theta + p(\cos\theta)\sin^2\theta + q(\cos\theta)\sin\theta \tag{24}$$

is an ϵ-approximation to f. □

Remark. *If $p(x)$ is a polynomial, it is easy to verify that $p(\cos\theta)$ is a trigonometric polynomial due to the fact* $\cos^n\theta = \sum_{k=0}^{n} \frac{\binom{n}{k}}{2^n} \cos((n-2k)\theta)$.

Prior to proving Theorem 1, we need to establish the following lemmas.

Lemma 5. *Sine is a Tauber-Wiener function.*

Proof. Assuming the interval to be $[0, \pi]$ first. For every continuous function f on $[0, \pi]$ and any $\epsilon > 0$, we can extend f to a continuous function F on $[0, 2\pi]$ so that $F(x) = f(x)$ on $[0, \pi]$ and $F(2\pi) = F(0)$. By Corollary 4.1, there exists a trigonometric polynomial

$$p(x) = a_0 + \sum_{n=1}^{N} a_n \cos(nx) + b_n \sin(nx) \tag{25}$$

such that

$$\sup_{x\in[0,\pi]} |f(x) - p(x)| \leq \sup_{x\in[0,2\pi]} |F(x) - p(x)| < \epsilon. \tag{26}$$

Let $c_0 = a_0$, $\lambda_0 = 0$, $\theta_0 = \frac{\pi}{2}$, $c_{2n-1} = b_n$, $\lambda_{2n-1} = n$, $\theta_{2n-1} = 0$, $c_{2n} = a_n$, $\lambda_{2n} = n$, $\theta_{2n} = \frac{\pi}{2}$, for $n = 1, 2, \ldots, N$, $p(x)$ is redefined as

$$p(x) = \sum_{i=0}^{2N} c_i \sin(\lambda_i x + \theta_i). \tag{27}$$

Thus we have

$$\left| f(x) - \sum_{i=0}^{2N} c_i \sin(\lambda_i x + \theta_i) \right| < \epsilon \tag{28}$$

for $x \in [0, \pi]$. Now consider a continuous function g on $[a, b]$, define $f(x) \in C[0, \pi] := g\left(\frac{b-a}{\pi}x + a\right)$, then by Eq. (28), we have

$$\left| g(x) - \sum_{i=0}^{2N} c_i \sin\left(\frac{\pi\lambda_i}{b-a}x - \frac{\pi\lambda_i a}{b-a} + \theta_i\right) \right| < \epsilon \tag{29}$$

holds for all $x \in [a, b]$. Thecrefore, it follows that for any continuous function g on $[a, b]$ and any $\epsilon > 0$, we can approximate g within ϵ by choosing N sufficiently large and adjusting c_i, λ_i, θ_i accordingly. Hence, the set of all such linear combinations of $\sin(x)$ is dense in $C[a, b]$, confirming that $\sin(x)$ is a Tauber-Wiener function. □

Remark. *It is straightforward to conclude that all sinusoidal functions are Tauber-Wiener functions.*

Lemma 6. *Suppose that $V_1 \subseteq X_1$, $V_2 \subseteq X_2$ are two compact sets in Banach spaces X_1 and X_2, respectively, then their Cartesian product $V_1 \times V_2$ is also compact.*

Proof. For every sequence $\left\{x_n^1, x_n^2\right\}$ in $V_1 \times V_2$, since V_1 is compact, $\left\{x_n^1\right\}$ has a subsequence $\left\{x_{n_k}^1\right\}$ that converges to some element $x^1 \in V_1$. As well, since V_2 is compact, there exists a subsequence $\left\{x_{n_k}^2\right\}$ that converges to $x^2 \in V_2$. It follows that $\left\{x_n^1, x_n^2\right\}$ converges to $\left(x^1, x^2\right) \in V_1 \times V_2$, thus $V_1 \times V_2$ is compact. □

Lemma 7. *Suppose that X is a Banach space, $K_1 \subseteq X_1$, $K_2 \subseteq X_2$ are two compact sets in X_1 and X_2, respectively. $\mathcal{U}$ is a compact set in $C(K_1)$, then the range $G(\mathcal{U})$ of the continuous operator G from $\mathcal{U}$ to $C(K_2)$ is compact in $C(K_2)$.*

Proof. For every sequence $\{f_n\}$ in $\mathcal{U}$, since $\mathcal{U}$ is compact, there exists a subsequence $\{f_{n_k}\}$ that converges to some function $f \in \mathcal{U}$. Since G is continuous, the convergence $f_{n_k} \to f$ in $C(K_1)$ implies

$$G(f_{n_k}) \to G(f) \quad \text{in} \quad C(K_2). \tag{30}$$

Thus, for every sequence $\{G(f_n)\}$ in $G(\mathcal{U})$, there exists a subsequence $\{G(f_{n_k})\}$ that converges to $G(f) \in G(\mathcal{U})$. Thecrefore, the range $G(\mathcal{U})$ of the continuous operator G is compact in $C(K_2)$. □

C.2 Universal Approximation Theorem for SepONet

Theorem 8 (Universal Approximation Theorem for Separable Operator Networks)**.** *Suppose that $\sigma \in (\mathrm{TW})$, g is a sinusoidal function, X is a Banach Space, $K \subseteq X$, $K_1 \subseteq \mathbb{R}^{d_1}$ and $K_2 \subseteq \mathbb{R}^{d_2}$ are three compact sets in X, $\mathbb{R}^{d_1}$ and $\mathbb{R}^{d_2}$, respectively, $\mathcal{U}$ is a compact set in $C(K)$, G is a nonlinear continuous operator, which maps $\mathcal{U}$ into a compact set $\mathcal{S} \subseteq C(K_1 \times K_2)$, then for any $\epsilon > 0$, there are positive integers n, r, m, constants c_i^k, ζ_k^1, ζ_k^2, ξ_{ij}^k, $\theta_i^k \in \mathbb{R}$, points $\omega_k^1 \in \mathbb{R}^{d_1}$, $\omega_k^2 \in \mathbb{R}^{d_2}$, $x_j \in K_1$, $i = 1, \ldots, n$, $k = 1, \ldots, r$, $j = 1, \ldots, m$, such that*

$$\left| G(u)(y) - \sum_{k=1}^{r} \sum_{i=1}^{n} c_i^k \sigma \left(\sum_{j=1}^{m} \xi_{ij}^k u\left(x_j\right) + \theta_i^k \right) g\left(w_k^1 \cdot y_1 + \zeta_k^1\right) g\left(w_k^2 \cdot y_2 + \zeta_k^2\right) \right| < \epsilon \tag{31}$$

holds for all $u \in \mathcal{U}$, $y = (y_1, y_2) \in K_1 \times K_2$.

Proof. Without loss of generality, we can assume that g is sine function, by Lemma 5, we have $g \in (TW)$; From the assumption that K_1 and K_2 are compact, by Lemma 6, $K_1 \times K_2$ is compact; Since G is a continuous operator that maps $\mathcal{U}$ into $C(K_1 \times K_2)$, it follows that the range $G(\mathcal{U}) = \{G(u) : u \in \mathcal{U}\}$ is compact in $C(K_1 \times K_2)$ due to Lemma 7; Thus by Theorem 2, for any $\epsilon > 0$, there exists a positive integer N, real numbers $c_k(G(u))$ and ζ_k, vectors $\omega_k \in R^{d_1+d_2}$, $k = 1, \ldots, N$, such that

$$\left| G(u)(y) - \sum_{k=1}^{N} c_k(G(u)) g\left(\omega_k \cdot y + \zeta_k\right) \right| < \frac{\epsilon}{2} \tag{32}$$

holds for all $y \in K_1 \times K_2$ and $u \in C(K)$. Let $(\omega_k^1, \omega_k^2) = \omega_k$, where $\omega_k^1 \in \mathbb{R}^{d_1}$ and $\omega_k^2 \in \mathbb{R}^{d_2}$. Utilizing the trigonometric angle addition formula, we have

$$g\left(\omega_k \cdot y + \zeta_k\right) = g\left(\omega_k^1 \cdot y_1 + \zeta_k\right) g\left(\omega_k^2 \cdot y_2 + \frac{\pi}{2}\right) + g\left(\omega_k^1 \cdot y_1 + \zeta_k + \frac{\pi}{2}\right) g\left(\omega_k^2 \cdot y_2\right). \tag{33}$$

Let $r = 2N$, $c_{N+k}(G(u)) = c_k(G(u))$, $\omega_{N+k}^1 = \omega_k^1$, $\omega_{N+k}^2 = \omega_k^2$, $\zeta_k^1 = \zeta_k$, $\zeta_k^2 = \frac{\pi}{2}$ for $k = 1, \ldots, N$, and let $\zeta_k^1 = \zeta_k + \frac{\pi}{2}$, $\zeta_k^2 = 0$ for $k = N+1, \ldots, r$, Eq. (32) can be expressed as:

$$\left| G(u)(y) - \sum_{k=1}^{r} c_k(G(u)) g\left(\omega_k^1 \cdot y_1 + \zeta_k^1\right) g\left(\omega_k^2 \cdot y_2 + \zeta_k^2\right) \right| < \frac{\epsilon}{2}. \tag{34}$$

Since G is a continuous operator, according to the last proposition of Theorem 2, we conclude that for each $k = 1, \ldots, 2N$, $c_k(G(u))$ is a continuous functional defined on $\mathcal{U}$. Repeatedly applying

Theorem 3, for each $k = 1, \ldots, 2N$, $c_k(G(u))$, we can find positive integers n_k,m_k, constants c_i^k, ξ_{ij}^k, $\theta_i^k \in R$ and $x_j \in K_1$, $i = 1, \ldots, n_k$, $j = 1, \ldots, m_k$, such that

$$\left| c_k(G(u)) - \sum_{i=1}^{n_k} c_i^k \sigma \left(\sum_{j=1}^{m_k} \xi_{ij}^k u(x_j) + \theta_i^k \right) \right| < \frac{\epsilon}{2L} \tag{35}$$

holds for all $k = 1, \ldots, r$ and $u \in \mathcal{U}$, where

$$L = \sum_{k=1}^{r} \sup_{y_1 \in K_2, y_2 \in K_3} \left| g\left(\omega_k^1 \cdot y_1 + \zeta_k^1\right) g\left(\omega_k^2 \cdot y_2 + \zeta_k^2\right) \right|. \tag{36}$$

Substituting Eq. (35) into Eq. (34), we obtain that

$$\left| G(u)(y) - \sum_{k=1}^{r} \sum_{i=1}^{n_k} c_i^k \sigma \left(\sum_{j=1}^{m_k} \xi_{ij}^k u\left(x_j\right) + \theta_i^k \right) g\left(w_k^1 \cdot y_1 + \zeta_k^1\right) g\left(w_k^2 \cdot y_2 + \zeta_k^2\right) \right| < \epsilon \tag{37}$$

holds for all $u \in \mathcal{U}$, $y_1 \in K_1$ and $y_2 \in K_2$. Let $n = \max_k n_k$, $m = \max_k m_k$. For all $n_k < i \leq n$, let $c_i^k = 0$. For all $m_k < j \leq m$, let $\xi_{ij}^k = 0$. Then Eq. (37) can be rewritten as:

$$\left| G(u)(y) - \sum_{k=1}^{r} \sum_{i=1}^{n} c_i^k \sigma \left(\sum_{j=1}^{m} \xi_{ij}^k u\left(x_j\right) + \theta_i^k \right) g\left(w_k^1 \cdot y_1 + \zeta_k^1\right) g\left(w_k^2 \cdot y_2 + \zeta_k^2\right) \right| < \epsilon, \tag{38}$$

which holds for all $u \in \mathcal{U}$, $y_1 \in K_1$ and $y_2 \in K_2$. This completes the proof of Theorem 1.

□

D PDE Problem Definitions, Training details, and Complete Test Results

D.1 PDE Problem Definitions

All PDE test problems exhibited in Section 3 are described in the subsections below.

D.1.1 Diffusion-Reaction Systems

Consider the following nonlinear diffusion-reaction system with a source term $u(x)$:

$$\frac{\partial s}{\partial t} = D \frac{\partial^2 s}{\partial x^2} + k s^2 + u(x), \quad (x, t) \in (0, 1) \times (0, 1] \tag{39}$$

with zero initial and boundary conditions, where $D = 0.01$ is the diffusion coefficient and $k = 0.01$ is the reaction rate. The input training source terms are sampled from a mean-zero Gaussian random field (GRF) (39) with a length scale 0.2. To generate the test dataset, we sample 100 different source terms from the same GRF and apply a second-order implicit finite difference method (13) to obtain the reference solutions on a uniform 128×128 grid.

D.1.2 Advection equation

Consider the following linear advection equation parameterized by the variable coefficients $u(x)$:

$$\frac{\partial s}{\partial t} + u(x) \frac{\partial s}{\partial x} = 0, \quad (x, t) \in (0, 1) \times (0, 1) \tag{40}$$

with the initial and boundary condition

$$\begin{aligned} s(x, 0) &= \sin(\pi x), \quad x \in (0, 1), \\ s(0, t) &= \sin\left(\frac{\pi}{2} t\right), \quad t \in (0, 1). \end{aligned} \tag{41}$$

The input training variable coefficients are strictly positive by defining $u(x) = v(x) - \min_x v(x) + 1$, where v is sampled from a GRF with length scale 0.2. To create the test dataset, we generate 100 new coefficients in the same manner that are not used in training and apply the Lax–Wendroff scheme (13) to solve the advection equation on a uniform 128×128 grid.

D.1.3 Burgers' Equation

Consider the nonlinear Burgers' equation:

$$\begin{aligned} &\frac{\partial s}{\partial t} + s\frac{\partial s}{\partial x} - \nu\frac{\partial^2 s}{\partial x^2} = 0, \quad (x,t) \in (0,1) \times (0,1], \\ &s(x,0) = u(x), \quad x \in (0,1) \end{aligned} \tag{42}$$

with periodic boundary conditions:

$$\begin{aligned} &s(0,t) = s(1,t), \\ &\frac{\partial s}{\partial x}(0,t) = \frac{\partial s}{\partial x}(1,t), \end{aligned} \tag{43}$$

where $t \in (0,1)$ and $\nu = 0.01$ is the viscosity. The input training initial conditions are sampled from a GRF $\sim \mathcal{N}\left(0, 25^2\left(-\Delta + 5^2 I\right)^{-4}\right)$ using the Chebfun package (7), satisfying the periodic boundary conditions. Synthetic test dataset consists of 100 unseen initial functions and their corresponding solutions, which are generated from the same GRF and are solved by spectral method on a 101×101 uniform grid using the spinOp library (35), respectively.

D.1.4 2D Nonlinear diffusion equation

Consider the 2D nonlinear diffusion equation which was used in (6):

$$\begin{aligned} &\frac{\partial s}{\partial t} = \alpha \nabla \cdot (s \nabla s), \quad (\boldsymbol{x}, t) \in \Omega \times [0,1], \\ &s(\boldsymbol{x}, 0) = u(\boldsymbol{x}), \quad \boldsymbol{x} \in \Omega, \\ &s(\boldsymbol{x}, t) = 0, \quad (\boldsymbol{x}, t) \in \partial\Omega \times [0,1], \end{aligned} \tag{44}$$

where $\boldsymbol{x} = (x, y)$ denotes 2D spatial variables, $\Omega = [0,1]^2$ is the spatial domain and $\alpha = 0.05$ is the diffusivity. The input training initial conditions are generated as a sum of Gaussian functions, parameterized as:

$$u(x,y) = \sum_{i=1}^{3} A_i \exp[-w_i\{(x - x_i)^2 + (y - y_i)^2\}], \tag{45}$$

where $A_i \sim \mathcal{U}(0.2, 0.5)$ are amplitudes, $w_i \sim \mathcal{U}(10, 20)$ are width parameters, and $(x_i, y_i) \sim \mathcal{U}(-0.5, 0.5)^2$ are center coordinates. We also generate 100 unseen test initial conditions using this method. The nonlinear diffusion equation is then solved using explicit Adams method to obtain reference solutions on a uniform 101×101 spatial grid with 101 time points.

D.2 Training details and hyperparameters

Both PI-DeepONet and SepONet were trained by minimizing the physics loss (Eq. (6)) using gradient descent with the Adam optimizer (18). The initial learning rate is 1×10^{-3} and decays by a factor of 0.9 every 1,000 iterations. Additionally, we resample input training functions and training points (including residual, initial, and boundary points) every 100 iterations.

Across all benchmarks and on both models (SepONet and PI-DeepONet), we apply Tanh activation for the branch net and Sine activation for the trunk net. We note that no extensive hyperparameter tuning was performed for either PI-DeepONet or SepONet. The code in this study is implemented using JAX and Equinox libraries (2; 17), and all training was performed on a single NVIDIA A100 GPU with 80 GB of memory. Training hyperparameters are provided in Table 2.

D.3 Additional SepONet results for Burgers' equation

SepONet's capabilities extend even further, as shown in Table 3. For the Burgers' equation, it achieves a 4.12% error with $N_c = 512^2$ and $N_f = 800$, while maintaining reasonable memory usage (10.485 GB) and training time (0.478 hours). These results underscore SepONet's ability to handle extreme-scale learning problems beyond PI-DeepONet's computational limits, making it valuable for complex, large-scale physical simulations.

Table 2: Training hyperparameters for different PDE benchmarks

Hyperparameters \ PDEs	Diffusion-reaction	Advection	Burgers'	2D Nonlinear diffusion
# of sensors	128	128	101	10201 (101 × 101)
Network depth	5	6	7	7
Network width	50	100	100	128
# of training iterations	50k	120k	80k	80k
Weight coefficients (λ_I / λ_b)	1 / 1	100 / 100	20 / 1	20 / 1

Table 3: Additional SepONet results for Burgers' equation, demonstrating that larger N_c and N_f can be used to enhance accuracy with minimal cost increase.

Metrics \ N_c & N_f	128^2 & 400	128^2 & 800	256^2 & 400	256^2 & 800	512^2 & 400	512^2 & 800
Relative ℓ_2 error (%)	6.60	6.21	5.68	4.46	5.38	4.12
Memory (GB)	0.966	1.466	2.466	4.466	5.593	10.485
Training time (hours)	0.0771	0.0957	0.1238	0.1717	0.2751	0.478

D.4 Complete test results

We report the relative ℓ_2 error, root mean squared error (RMSE), GPU memory usage and total training time as metrics to assess the performance of PI-DeepONet and SepONet. Specifically, the mean and standard deviation of the relative ℓ_2 error and RMSE are calculated over all functions in the test dataset. The complete test results are shown in Table 4 and Table 5.

Table 4: Performance comparison of PI-DeepONet and SepONet with varying number of training points (N_c) and fixed number of input training functions ($N_f = 100$). The '-' symbol indicates that results are not available due to out-of-memory issues.

Equations	Metrics	Models	8^d	16^d	32^d	64^d	128^d
Diffusion-Reaction $d = 2$	Relative ℓ_2 error (%)	PI-DeepONet	1.39 ± 0.71	1.11 ± 0.59	0.87 ± 0.41	0.83 ± 0.35	0.73 ± 0.34
		SepONet	1.49 ± 0.82	0.79 ± 0.35	0.70 ± 0.33	0.62 ± 0.28	0.62 ± 0.26
	RMSE ($\times 10^{-2}$)	PI-DeepONet	0.58 ± 0.29	0.46 ± 0.22	0.37 ± 0.20	0.36 ± 0.20	0.32 ± 0.18
		SepONet	0.62 ± 0.28	0.35 ± 0.22	0.32 ± 0.23	0.28 ± 0.20	0.29 ± 0.21
	Memory (GB)	PI-DeepONet	0.729	1.227	3.023	9.175	35.371
		SepONet	**0.715**	**0.717**	**0.715**	**0.717**	**0.719**
	Training time (hours)	PI-DeepONet	0.0433	0.0641	0.1497	0.7252	2.8025
		SepONet	**0.0403**	**0.0418**	**0.0430**	**0.0427**	**0.0326**
Advection $d = 2$	Relative ℓ_2 error (%)	PI-DeepONet	9.27 ± 1.94	7.55 ± 1.86	6.79 ± 1.84	6.69 ± 1.95	5.72 ± 1.57
		SepONet	14.29 ± 2.65	11.96 ± 2.17	6.14 ± 1.58	5.80 ± 1.57	4.99 ± 1.40
	RMSE ($\times 10^{-2}$)	PI-DeepONet	5.88 ± 1.34	4.79 ± 1.27	4.31 ± 1.23	4.24 ± 1.29	3.63 ± 1.05
		SepONet	9.06 ± 1.88	7.58 ± 1.55	3.90 ± 1.09	3.69 ± 1.07	3.17 ± 0.95
	Memory (GB)	PI-DeepONet	0.967	1.741	5.103	17.995	59.806
		SepONet	**0.713**	**0.715**	**0.715**	**0.715**	**0.719**
	Training time (hours)	PI-DeepONet	**0.0787**	0.1411	0.4836	2.3987	8.231
		SepONet	0.0843	**0.0815**	**0.0844**	**0.0726**	**0.0730**
Burgers' $d = 2$	Relative ℓ_2 error (%)	PI-DeepONet	29.33 ± 3.85	20.31 ± 4.31	14.17 ± 5.25	13.72 ± 5.59	-
		SepONet	29.42 ± 3.79	31.53 ± 3.44	28.74 ± 4.11	11.85 ± 4.06	7.51 ± 4.04
	RMSE ($\times 10^{-2}$)	PI-DeepONet	4.19 ± 2.79	2.82 ± 1.86	2.23 ± 2.10	2.20 ± 2.13	-
		SepONet	4.18 ± 2.74	4.44 ± 2.81	4.11 ± 2.76	1.80 ± 1.60	1.23 ± 1.44
	Memory (GB)	PI-DeepONet	1.253	2.781	5.087	18.001	-
		SepONet	**0.603**	**0.605**	**0.603**	**0.605**	**0.716**
	Training time (hours)	PI-DeepONet	0.1497	0.2375	0.6431	3.2162	-
		SepONet	**0.0706**	**0.0719**	**0.0716**	**0.0718**	**0.0605**
Nonlinear diffusion $d = 3$	Relative ℓ_2 error (%)	PI-DeepONet	17.38 ± 5.56	9.90 ± 2.91	-	-	-
		SepONet	16.10 ± 4.46	12.11 ± 3.89	6.81 ± 1.98	6.73 ± 1.96	6.44 ± 1.69
	RMSE ($\times 10^{-2}$)	PI-DeepONet	1.86 ± 0.62	1.04 ± 0.23	-	-	-
		SepONet	1.72 ± 0.49	1.29 ± 0.37	0.72 ± 0.19	0.71 ± 0.17	0.68 ± 0.15
	Memory (GB)	PI-DeepONet	6.993	37.715	-	-	-
		SepONet	**3.471**	**2.897**	**2.899**	**2.897**	**13.139**
	Training time (hours)	PI-DeepONet	0.5836	6.6399	-	-	-
		SepONet	**0.1044**	**0.1069**	**0.1056**	**0.1456**	**0.5575**

Table 5: Performance comparison of PI-DeepONet and SepONet with varying number of input training functions (N_f) and fixed number of training points ($N_c = 128^d$, d indicated by problem instance). The '-' symbol indicates that results are not available due to out-of-memory issues.

Equations	Metrics	Models	5	10	20	50	100
Diffusion-Reaction $d = 2$	Relative ℓ_2 error (%)	PI-DeepONet	34.54 ± 27.83	4.23 ± 2.52	1.72 ± 1.00	0.91 ± 0.46	0.73 ± 0.34
		SepONet	22.40 ± 12.30	3.11 ± 1.89	1.19 ± 0.74	0.73 ± 0.32	0.62 ± 0.26
	RMSE ($\times 10^{-2}$)	PI-DeepONet	14.50 ± 9.04	1.75 ± 0.90	0.71 ± 0.37	0.40 ± 0.28	0.32 ± 0.18
		SepONet	9.34 ± 5.37	1.36 ± 1.07	0.50 ± 0.29	0.34 ± 0.25	0.29 ± 0.21
	Memory (GB)	PI-DeepONet	2.767	5.105	9.239	17.951	35.371
		SepONet	**0.719**	**0.719**	**0.717**	**0.717**	**0.719**
	Training time (hours)	PI-DeepONet	0.1268	0.2218	0.5864	1.4018	2.8025
		SepONet	**0.0375**	**0.0390**	**0.0370**	**0.0317**	**0.0326**
Advection $d = 2$	Relative ℓ_2 error (%)	PI-DeepONet	9.64 ± 2.91	8.77 ± 2.23	7.57 ± 1.98	6.69 ± 1.93	5.72 ± 1.57
		SepONet	7.62 ± 2.06	6.59 ± 1.71	5.47 ± 1.57	5.18 ± 1.51	4.99 ± 1.40
	RMSE ($\times 10^{-2}$)	PI-DeepONet	6.11 ± 1.90	5.55 ± 1.51	4.80 ± 1.33	4.24 ± 1.28	3.63 ± 1.05
		SepONet	4.83 ± 1.38	4.18 ± 1.17	3.47 ± 1.06	3.29 ± 1.02	3.17 ± 0.95
	Memory (GB)	PI-DeepONet	3.021	5.611	9.707	34.511	59.806
		SepONet	**0.713**	**0.715**	**0.719**	**0.719**	**0.719**
	Training time (hours)	PI-DeepONet	0.3997	1.0766	1.9765	4.411	8.231
		SepONet	**0.0754**	**0.0715**	**0.0736**	**0.0720**	**0.0730**
Burgers' $d = 2$	Relative ℓ_2 error (%)	PI-DeepONet	28.48 ± 4.17	28.63 ± 4.10	28.26 ± 4.38	12.33 ± 5.14	-
		SepONet	27.79 ± 4.40	28.16 ± 4.24	22.78 ± 6.47	10.25 ± 4.44	7.51 ± 4.04
	RMSE ($\times 10^{-2}$)	PI-DeepONet	4.09 ± 2.77	4.11 ± 2.78	4.07 ± 2.78	1.96 ± 1.92	-
		SepONet	4.01 ± 2.75	4.05 ± 2.76	3.30 ± 2.55	1.65 ± 1.64	1.23 ± 1.44
	Memory (GB)	PI-DeepONet	5.085	9.695	17.913	35.433	-
		SepONet	**0.605**	**0.607**	**0.607**	**0.609**	**0.716**
	Training time (hours)	PI-DeepONet	0.5135	1.3896	2.6904	5.923	-
		SepONet	**0.0725**	**0.0707**	**0.0703**	**0.0612**	**0.0605**
Nonlinear diffusion $d = 3$	Relative ℓ_2 error (%)	PI-DeepONet	-	-	-	-	-
		SepONet	31.94 ± 9.18	25.48 ± 8.95	21.16 ± 7.82	10.21 ± 3.31	6.44 ± 1.69
	RMSE ($\times 10^{-2}$)	PI-DeepONet	-	-	-	-	-
		SepONet	3.44 ± 1.13	2.73 ± 0.99	2.27 ± 0.91	1.09 ± 0.32	0.68 ± 0.15
	Memory (GB)	PI-DeepONet	-	-	-	-	-
		SepONet	**2.923**	**3.139**	**4.947**	**6.995**	**13.139**
	Training time (hours)	PI-DeepONet	-	-	-	-	-
		SepONet	**0.1175**	**0.1408**	**0.1849**	**0.3262**	**0.5575**

E Complete solution to separation of variables example Eq. (9)

Recall the linear PDE system treated in Appendix A.3:

$$\mathcal{M}[t]s(y) = \mathcal{L}_1[y_1]s(y) + \cdots + \mathcal{L}_d[y_d]s(y), \tag{46}$$

where $\mathcal{M}[t] = \frac{d}{dt} + h(t)$ is a first order differential operator of t, and $\mathcal{L}_1[y_1], ..., \mathcal{L}_d[y_d]$ are linear second order ordinary differential operators of their respective variables $y_1, ..., y_d$ only. Furthermore, assume we are provided Robin boundary conditions in each variable and separable initial condition $s(t = 0, y_1, \ldots, y_d) = \prod_{n=1}^{d} \phi_n(y_n)$ for functions $\phi_n(y_n)$ that satisfy the boundary conditions.

Assuming a separable solution exists, $s(y) = T(t)Y_1(y_1) \cdots Y_d(y_d)$, the PDE can be decomposed in the following form:

$$\frac{\mathcal{M}T(t)}{T(t)} = \frac{\mathcal{L}_1 Y_1(y_1)}{Y_1(y_1)} + \cdots + \frac{\mathcal{L}_d Y_d(y_d)}{Y_d(y_d)}, \tag{47}$$

where it is apparent that each term in the sequence is a constant, since they are each only functions of a single variable. Consequently, we may solve each of the $\mathcal{L}_n$ terms independently using Sturm-Liouville theory. After we have found the associated eigenfunctions ($Y_n^{k_n}$) and eigenvalues ($\lambda_n^{k_n}$), we may manually integrate the left-hand side. Finally, we may decompose the separable initial condition into a product of sums of the orthonormal basis functions (eigenfunctions) of each variable. The

resulting solution is given by

$$
\begin{aligned}
s(y) = s(t, y_1, \ldots, y_d) &= \sum_{k=(k_1,\ldots,k_d)} B_k T^k(t) \prod_{n=1}^{d} Y_n^{k_n}(y_n), \\
T^k(t) &\coloneqq T^{(k_1,\ldots,k_d)}(t) = \exp\left(-\int_0^t h(\tau) d\tau + t \sum_{n=1}^{d} \lambda_n^{k_n} \right), \\
B_k \coloneqq B_{(k_1,\ldots,k_d)} &= \prod_{n=1}^{d} \frac{\langle Y_n^{k_n}(y_n), \phi_n(y_n) \rangle_n}{\langle Y_n^{k_n}(y_n), Y_n^{k_n}(y_n) \rangle_n}, \quad \lambda_n^{k_n} = \frac{\mathcal{L}_n Y_n^{k_n}(y_n)}{Y_n^{k_n}(y_n)}, \\
& n = 1, ..., d, \quad k_n = 1, 2, \ldots, \infty.
\end{aligned}
\tag{48}
$$

Here, $k = (k_1, \ldots, k_d)$, where $k_n \in \{1, 2, ..., \infty\}, \forall n \in \{1, ..., d\}$, is a lumped index that counts over all possible products of eigenfunctions $Y_n^{k_n}$ with associated eigenvalues $\lambda_n^{k_n}$. $\langle \cdot \rangle_n$ is an appropriate inner product associated with the separated Hilbert space of the $\mathcal{L}_n$-th operator. To obtain Eq. (9) in the main manuscript, one only need to break up the sum over all k_n indices into a single ordered index.

F Linear Heat Equation Example

SepONet is motivated by the classical method of separation of variables, which is often employed to solve linear partial differential equations (PDEs). To illustrate the connection between these approaches, consider the linear heat equation:

$$
\begin{aligned}
&\frac{\partial s}{\partial t} = \frac{1}{\pi^2} \frac{\partial^2 s}{\partial x^2}, \quad (x, t) \in (0, 1) \times (0, 1], \\
&s(x, 0) = u(x), \quad x \in (0, 1), \\
&s(0, t) = s(1, t) = 0, \quad t \in (0, 1).
\end{aligned}
\tag{49}
$$

The goal is to solve this equation for various initial conditions u(x) using both the separation of variables technique and the SepONet method, allowing for an intuitive comparison between the two.

F.1 Separation of Variables Technique

We seek a solution in the form:

$$
s(x, t) = X(x)T(t) \tag{50}
$$

for functions X, T to be determined. Substituting Eq. (50) into Eq. (49) yields:

$$
\frac{X''}{X} = -\lambda \text{ and } \frac{\pi^2 T'}{T} = -\lambda \tag{51}
$$

for some constant λ. To satisfy the boundary condition, X must solve the following eigenvalue problem:

$$
\begin{aligned}
X''(x) + \lambda X(x) = 0, \quad x \in (0, 1), \\
X(0) = X(1) = 0,
\end{aligned}
\tag{52}
$$

and T must solve the ODE problem:

$$
T'(t) = -\frac{\lambda}{\pi^2} T(t). \tag{53}
$$

The eigenvalue problem Eq. (52) has a sequence of solutions:

$$
\lambda_k = (k\pi)^2, \quad X_k(x) = \sin(k\pi x), \quad \text{for } k = 1, 2, \ldots \tag{54}
$$

For any λ, the ODE solution for T is $T(t) = Ae^{-\frac{\lambda}{\pi^2} t}$ for some constant A. Thus, for each eigenfunction X_k with corresponding eigenvalue λ_k, we have a solution T_k such that the function

$$
s_k(x, t) = X_k(x) T_k(t) \tag{55}
$$

will be a solution of Eq. (51). In fact, an infinite series of the form

$$s(x,t) = \sum_{k=1}^{\infty} X_k(x)T_k(t) = \sum_{k=1}^{\infty} A_k e^{-k^2 t} \sin(k\pi x) \tag{56}$$

will also be a solution satisfying the differential operator and boundary condition of the heat equation Eq. (49) subject to appropriate convergence assumptions of this series. Now let $s(x,0) = u(x)$, we can find coefficients:

$$A_k = 2\int_0^1 \sin(k\pi x)\, u(x) dx \tag{57}$$

such that Eq. (56) is the exact solution of the heat equation Eq. (49).

F.2 SepONet Method

In this section, we apply the SepONet framework to solve the linear heat equation Eq. (49) and compare the basis functions it learns with those derived from the classical separation of variables method. Recall that a SepONet, parameterized by $\boldsymbol{\theta}$, approximates the solution operator of Eq. (49) as follows:

$$G_{\boldsymbol{\theta}}(u)(x,t) = \sum_{k=1}^{r} \beta_k(u(x_1), u(x_2), \ldots, u(x_{128}))\tau_k(t)\zeta_k(x), \tag{58}$$

where $x_1, x_2, \ldots, x_{128}$ are 128 equi-spaced sensors in $[0,1]$, β_k is the k-th output of the branch net, and the basis functions $\tau_k(t)$ and $\zeta_k(x)$ are the k-th outputs of two independent trunk nets.

Training settings The branch and trunk networks each have a width of 5 and a depth of 50. To determine the parameters $\boldsymbol{\theta}$, we trained SepONet for 80,000 iterations, minimizing the physics loss. Specifically, we set $\lambda_I = 20$, $\lambda_b = 1$, $N_f = 100$, and $N_c = 128^2$ in the physics loss. The training functions (initial conditions) $\left\{u^{(i)}\right\}_{i=1}^{N_f}$ were generated from a Gaussian random field (GRF) $\sim \mathcal{N}\left(0, 25^2\left(-\Delta + 5^2 I\right)^{-4}\right)$ using the Chebfun package (7), ensuring zero Dirichlet boundary conditions. Additional training settings are detailed in Appendix B.2 of the main text.

Evaluation We evaluated the model on 100 unseen initial conditions sampled from the same GRF, using the forward Euler method to obtain reference solutions on a 128×128 uniform spatio-temporal grid.

Impact of the rank r Since $\tau_k(t)$ and $\zeta_k(x)$ are independent of the initial condition u, learning an expressive and rich set of basis functions is crucial for SepONet to generalize to unseen initial conditions. To investigate the impact of the rank r on the generalization error, we trained SepONet with ranks ranging from 1 to 50. The mean RMSE between SepONet's predictions and the reference solutions over 100 unseen test initial conditions was reported. For comparison, we also computed the mean RMSE of the truncated analytical solution at rank r for r from 1 to 15. The results are presented in Fig. 4.

As r increases, the truncated analytical solution quickly converges to the reference solution. The nonzero RMSE arises due to numerical errors in computing the coefficients A_k and the inherent inaccuracies of the forward Euler method used to generate the reference solution. For SepONet, we observed that when $r = 1, 2$, the mean RMSE aligns closely with that of the truncated solution. However, as r increases beyond that point, the error decreases more gradually, stabilizing around $r = 50$. This indicates that SepONet may not necessarily learn the exact same basis functions as those from the truncated analytical solution. Instead, a higher rank r allows SepONet to develop its own set of basis functions, achieving similar accuracy to the truncated solution.

SepONet basis functions The learned basis functions for different ranks r are visualized in Fig. 5 to Fig. 9.

At $r = 1$, SepONet learns basis functions that closely resemble the first term of the truncated solution. For $r = 2$, the learned functions are quite similar to the first two terms of the truncated series. However, when $r = 5$, the basis functions diverge from the truncated solution series, although

some spatial components still resemble sinusoidal functions and the temporal components remain monotonic. As r increases further, SepONet continues to improve in accuracy, though the learned basis functions increasingly differ from the truncated series, confirming SepONet's ability to accurately approximate the solution using its own learned basis functions.

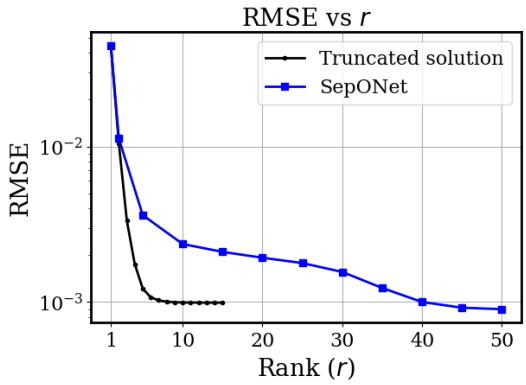

Figure 4: Comparison of RMSE between the truncated analytical solution and SepONet predictions for varying rank r. The truncated analytical solution quickly converges, while SepONet shows a slower decay in error, converging around $r = 50$.

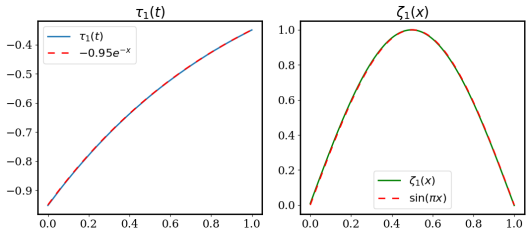

Figure 5: Learned basis functions $\tau_k(t)$ and $\zeta_k(x)$ for $r = 1$. SepONet learns the same basis functions as the first term of the truncated solution.

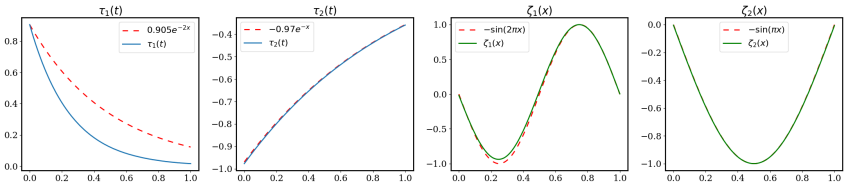

Figure 6: Learned basis functions $\tau_k(t)$ and $\zeta_k(x)$ for $r = 2$. SepONet learns very similar basis functions as the first two terms of the truncated solution.

G Visualization of SepONet Predictions

In this section, we showcase the performance of trained SepONets in predicting solutions for PDEs under previously unseen configurations. The SepONets were trained using $N_f = 100$ and $N_c = 128^d$, where d denotes the dimensionality of the PDE problem. The prediction results are presented in Figs. 10 to 13.

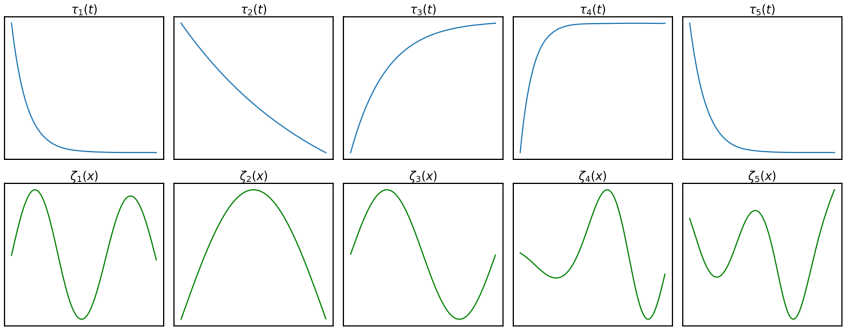

Figure 7: Learned basis functions $\tau_k(t)$ and $\zeta_k(x)$ for $r = 5$.

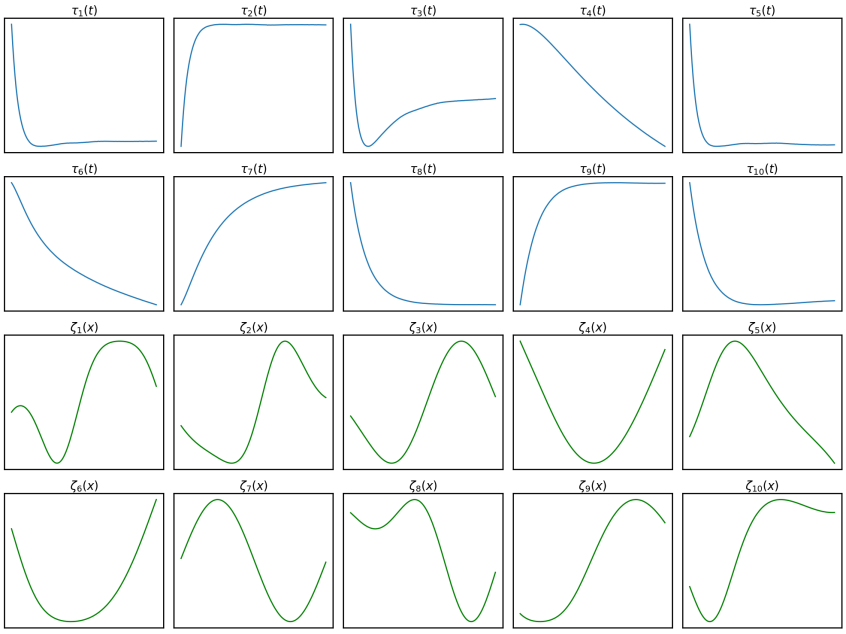

Figure 8: Learned basis functions $\tau_k(t)$ and $\zeta_k(x)$ for $r = 10$.

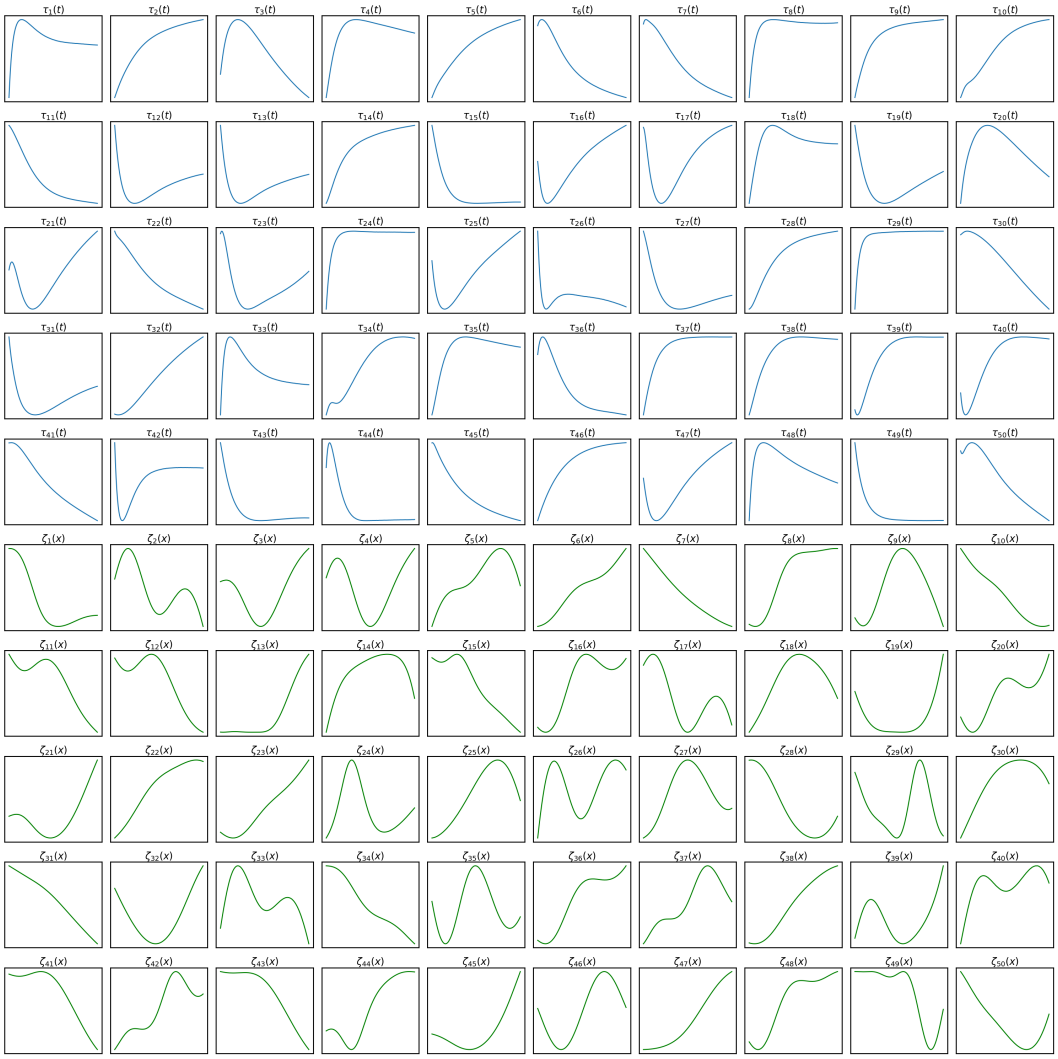

Figure 9: Learned basis functions $\tau_k(t)$ and $\zeta_k(x)$ for $r = 50$.

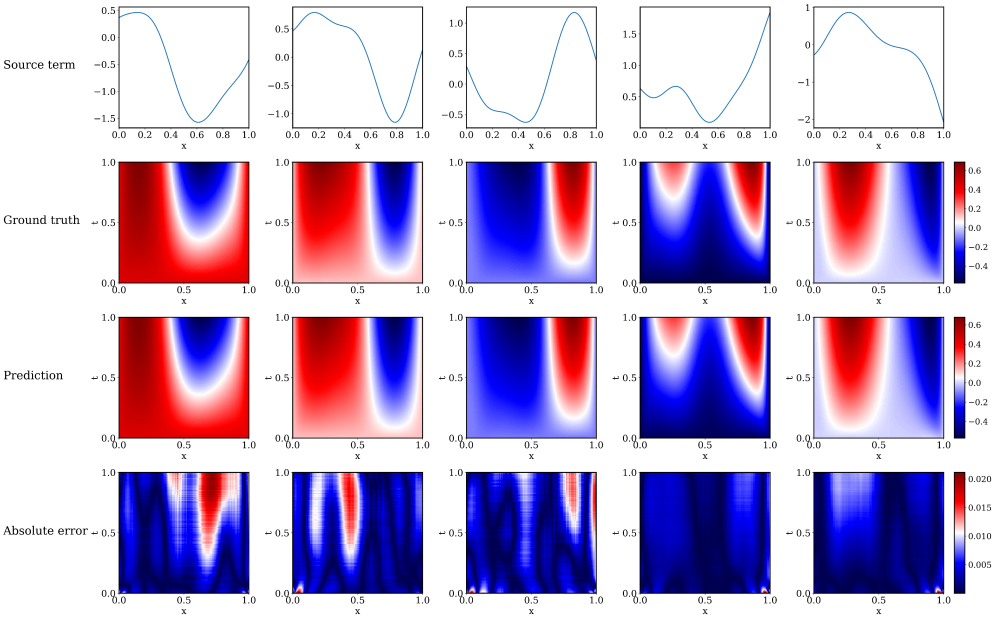

Figure 10: (1+1)-d Diffusion-reaction equation.

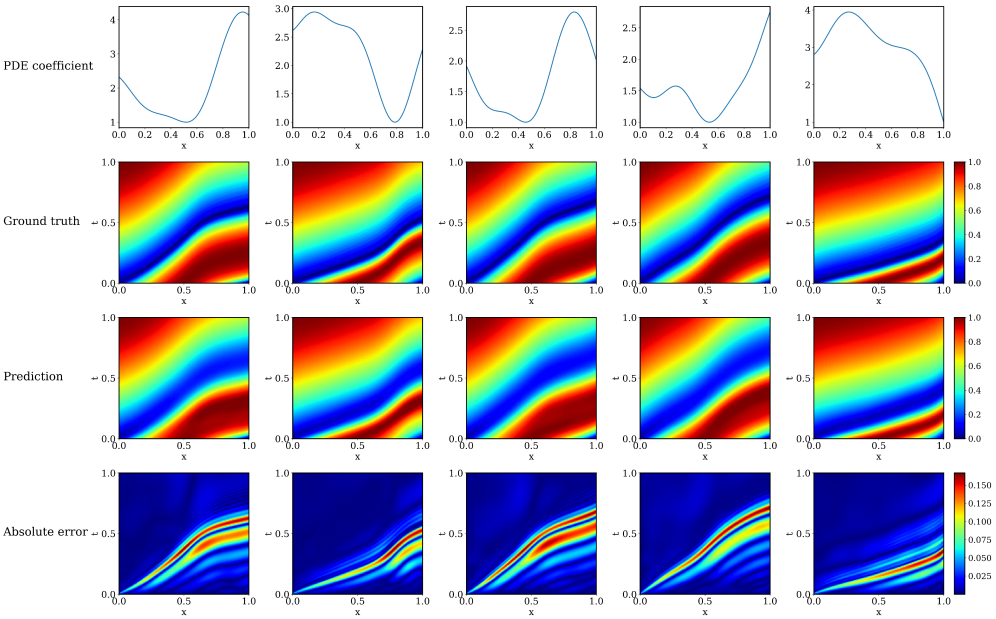

Figure 11: (1+1)-d Advection equation.

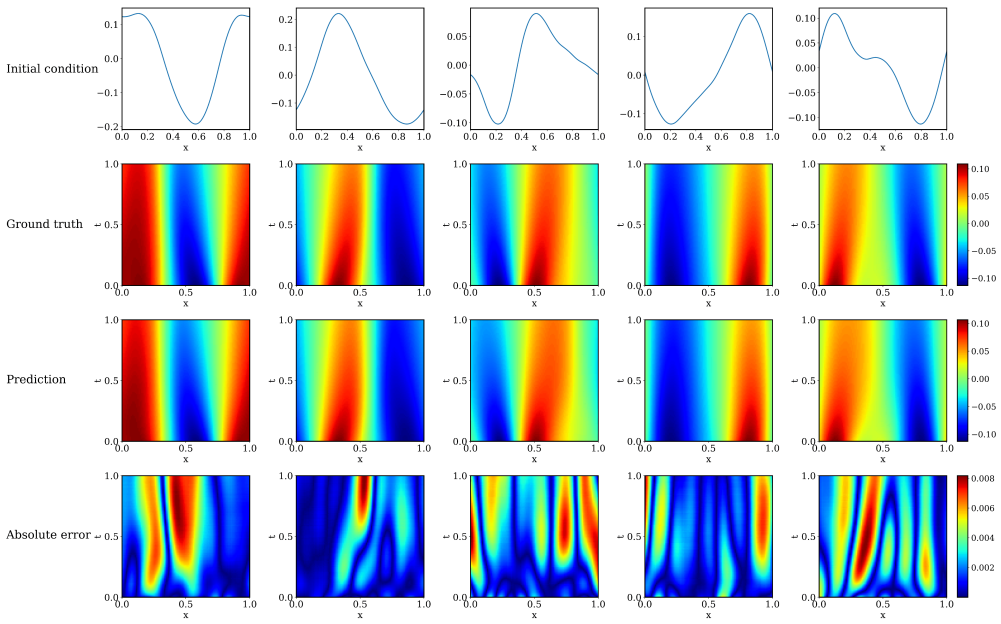

Figure 12: (1+1)-d Burgers' equation.

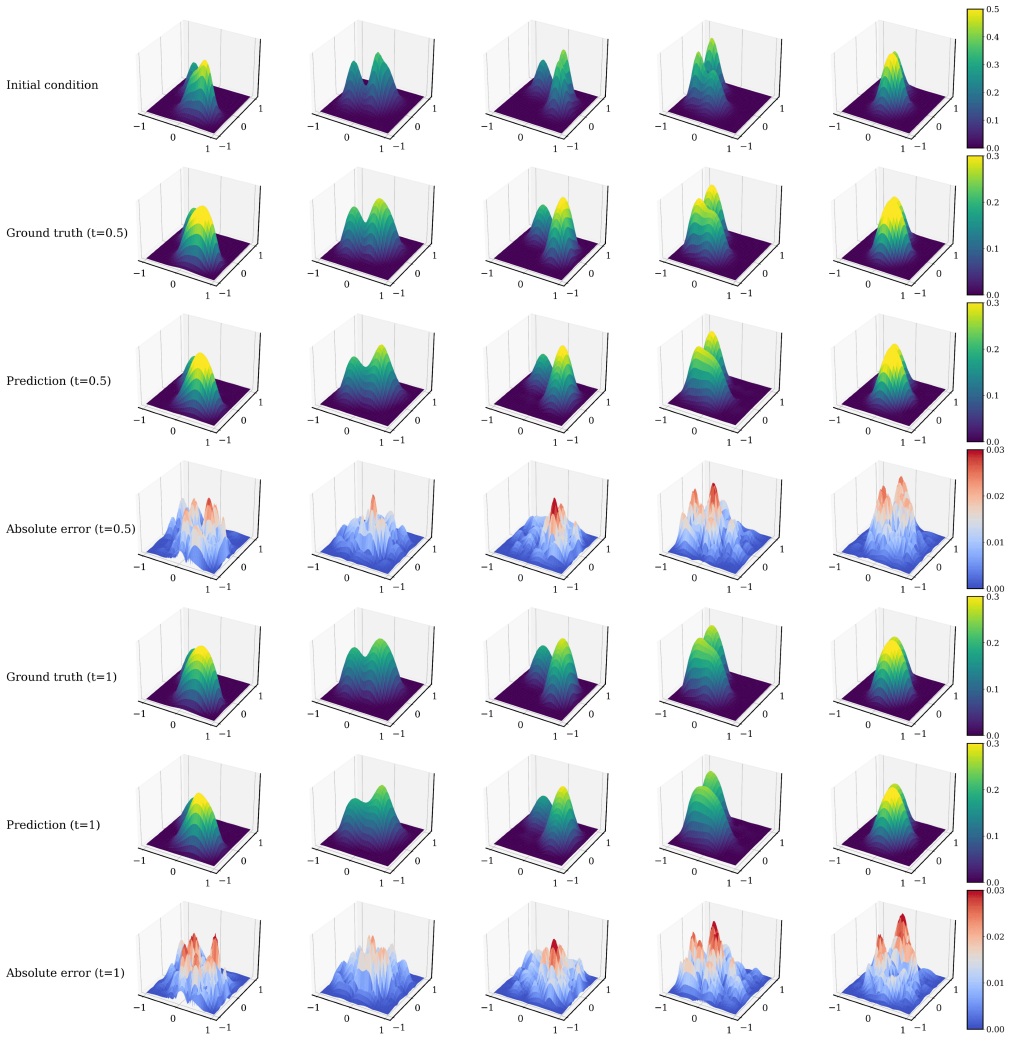

Figure 13: (2+1)-d Nonlinear diffusion equation. Two snapshots at $t = 0.5$ and $t = 1$ are presented.